Volume 58
Number 34
30 April 2022
Pages 5179–5306

ChemComm

Chemical Communications

rsc.li/chemcomm

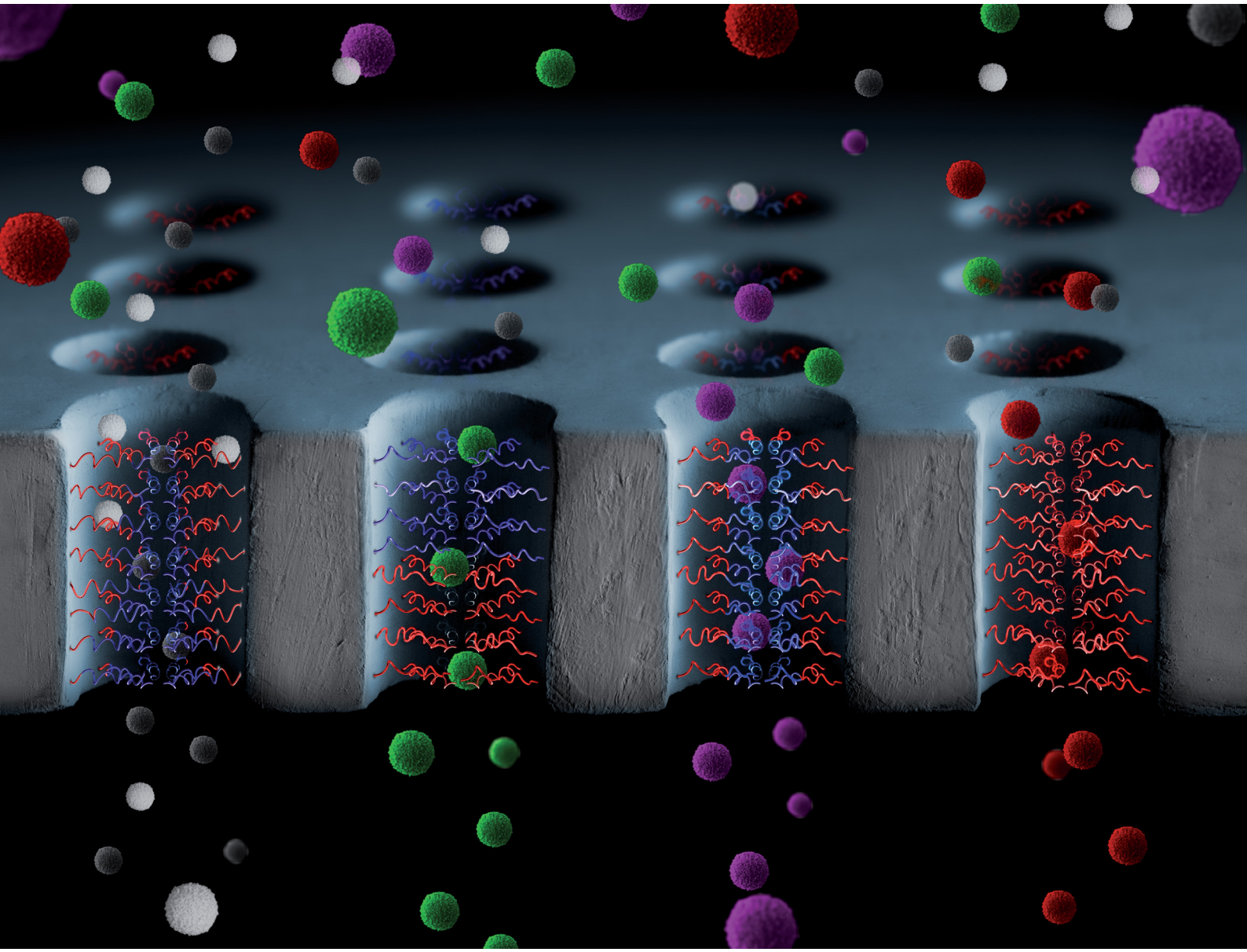

ISSN 1359-7345

ROYAL SOCIETY OF CHEMISTRY

FEATURE ARTICLE

Raheleh Pardehkhorram and Annette Andrieu-Brunsen
Pushing the limits of nanopore transport performance by polymer functionalization

ChemComm

ROYAL SOCIETY OF CHEMISTRY

FEATURE ARTICLE

View Article Online
View Journal | View Issue

Cite this: *Chem. Commun.*, 2022, **58**, 5188

Pushing the limits of nanopore transport performance by polymer functionalization

Raheleh Pardehkhorram and Annette Andrieu-Brunsen *

Inspired by the design and performance of biological pores, polymer functionalization of nanopores has emerged as an evolving field to advance transport performance within the last few years. This feature article outlines developments in nanopore functionalization and the resulting transport performance including gating based on electrostatic interaction, wettability and ligand binding, gradual transport controlled by polymerization as well as functionalization-based asymmetric nanopore and nanoporous material design going towards the transport direction. Pushing the limits of nanopore transport performance and thus reducing the performance gap between biological and technological pores is strongly related to advances in polymerization chemistry and their translation into nanopore functionalization. Thereby, the effect of the spatial confinement has to be considered for polymer functionalization as well as for transport regulation, and mechanistic understanding is strongly increased by combining experiment and theory. A full mechanistic understanding together with highly precise nanopore structure design and polymer functionalization is not only expected to improve existing application of nanoporous materials but also opens the door to new technologies. The latter might include out of equilibrium devices, ionic circuits, or machine learning based sensors.

Received 25th February 2022,
Accepted 25th March 2022

DOI: 10.1039/d2cc01164f

rsc.li/chemcomm

Macromolecular Chemistry, Smart Membranes, Technical University of Darmstadt, 64287 Darmstadt, Germany. E-mail: annette.andrieu-brunsen@tu-darmstadt.de

Raheleh Pardehkhorram

Raheleh Pardehkhorram received her BSc degree in Chemistry from the Ferdowsi University of Mashhad (Iran). She completed her MSc in inorganic chemistry from Iran University of Science and Technology. In 2015, she joined the PhD program in Chemistry under the supervision of Prof. Justin Gooding at the University of New South Wales (UNSW) Sydney. She then spent one year at UNSW Sydney as a postdoctoral fellow. Currently, she is working in the group of Prof. Annette Andrieu-Brunsen at the TU-Darmstadt (Germany). Her main research interest focuses on the design of plasmonic nanomaterials and advanced hybrid nanoporous composites for sensing and transport applications.

Annette Andrieu-Brunsen

Annette Andrieu-Brunsen studied Chemistry at the Philipps-Universität Marburg (Germany). She got her PhD from the Johannes-Gutenberg Universität and the Max-Planck-Institute for Polymer Research in Mainz (Germany) partly funded by the Studienstiftung des Deutschen Volkes in 2010 and has been working together with Prof. Soler-Illia and Prof. Azzaroni at the CNEA in Buenos Aires (Argentina) before being appointed as the Assistant Professor at the TU-Darmstadt (Germany). In 2018 she was appointed as an associate professor at TU-Darmstadt and in 2020 she was appointed as a full professor at TU Darmstadt (Germany). She received several awards and was granted an ERC StG in 2018. Her research interest focuses on functional nanopore and nanopore transport design. This includes polymer functionalization of spatially confined nanopores, nanopore wetting and charge control, innovative nanoporous material and architecture design as well as automated design procedures.

Introduction

Transport through nanopores is an essential aspect in many technologies ranging from chromatography and membrane-based separation to oil-production and catalysis.[1–7] Biological pores and channels often serve as inspiration as they facilitate highly selective, directed, gated in time and fast transport rates of molecules in nature. Three often-mentioned examples of biological pores and channels are the potassium channel[8] and the nuclear pore complex,[9] or aquaporin.[10] In an attempt to develop such smart and selective gating platforms using technological pores, integration of porous nanomaterials and polymers has emerged as a highly dynamic field. Such hybrid porous materials offer great potential for a wide range of applications from water management, and energy conversion, to drug delivery, sensing, protein separation, artificial molecular pumping, and ionic circuit integration.[4] Nanopore application is based on the combination of nanopore structure design, advances in nanopore functionalization, and hierarchical porous material architecture control. Thereby nanopore functionalization with polymers represents a versatile, and in the last approximately 15 years increasingly investigated, strategy. Polymer functionalized nanopores profit from the huge library of different, stimuli-responsive polymers and from the concept that multiple monomers are combined into one polymer chain which is, for example, end-grafted to the pore wall. This results in the possibility of multiplying and precisely adjusting functional density and functional composition in and along such a nanopore pre-defined from the pore wall.

Transport in such functionalized nanopores is strongly determined by the nanopore charge regulation and thus by the electrostatic interaction between the nanopore and the transported species, as well as by polarity or wettability, and by specific interaction or ligand binding. In addition to the simple homogeneously functionalized nanopore the local variation of structure and functionalization-encoded charge, polarity, and ligand binding is an additional parameter to achieve improved transport performance. The potential of asymmetric nanopore design within the nanopore dimension is also inspired by biological pores, and is nicely demonstrated by the structure of the potassium channel[8] or the nuclear pore complex.[9] While trying to use nanopore functionalization to tune nanopore transport it has to be considered that the pore wall curvature as well as the limited space with respect to the molecular size of transported species and with respect to the nanopore wall grafted polymers, often referred to as spatial confinement, strongly influences the nanopore performance.[11] In regard to molecular transport in polymer-functionalized nanopores, confinement effects are particularly discussed in the context of charge regulation but also in the context of ligand binding constants.[12] But not only the nanopore structure and its functionalization determine transport performance in polymer-functionalized nanopores. The solution composition and the interaction of dissolved molecules or ions with the grafted molecules or polymers within the nanopore have to be considered.[13] Besides the pore wall curvature, and the spatial confinement, these might significantly affect the subtle interplay of polymer conformational entropy, mixing entropy of mobile species and grafted polymer as well as the acid–base equilibrium in polyelectrolyte functionalized nanopores.[14,15] This is of special interest as soon as real applications are considered, as these usually require contact to solutions not just containing one specific molecule or salt. Mastering all these aspects experimentally and theoretically is an ongoing and fascinating challenge, potentially not only leading towards improved understanding and application but to the next level of complex nanopore-containing systems such as ionic circuits or autonomous sensors.[16–19]

Many different synthetic porous materials including metal organic frameworks (MOF), covalent organic frameworks (COF), graphene, zeolites, solid state nanopores, mesoporous materials, ceramic and polymer membranes, or even 2D-layered materials such as MXenes can be summarized under the term nanoporous materials. In this feature article we mainly refer to mesoporous ceramic materials fabricated using sol–gel chemistry using block-copolymer template self-assembly[20,21] as well as to solid state nanopores such as ion track etched nanopores. The term nanopore in this feature article is used as a general expression for a pore with a diameter of a few up to several tens of nanometres. According to IUPAC this spans from micropores (diameter below 2 nm), mesopores (diameter 2–50 nm) to macropores (diameter larger than 50 nm).[22] The majority of the discussed examples refer to mesopores using this IUPAC definition. Herein, we will mainly focus on ion or small molecule transport by nanopore design.

Insights into nanopore gating and confinement effects

Regarding molecular transport control, an important achievement is nanopore gating referring to opening and closing a nanopore for specific molecules upon a certain stimulus. While sieving by size is the most prominent separation mechanism applied in most technological membranes, gating is additionally dependent on nanopore charge, wettability, or ligand binding.[11,23,24] Various reviews on nanopore gating have been published within the last decade.[11,25–30] Inspired by biological pores showing selective, directed, fast and gated transport, many approaches to implement gating into technological nanopores by using material functionalization and design, especially using polymers, have been reported. Thereby gating based on electrostatic interaction, and thus switching the nanopore charge, is the most explored approach toward gated transport in nanopores. The reason for this might be that charged nanopores relatively easily result in electrostatic ion exclusion or ion preconcentration due to electrostatic interaction. Especially in case the pore diameter is of similar dimensions to the Debye Screening Length this electrostatic exclusion or attraction can be used for nanopore gating, *e.g.* upon changing pH in contact with pH-responsive polymer functionalized nanopores. Polymer grafting to achieve gating of nanopore accessibility is obtained by a variety of different

polymerization techniques although the majority of reports is based on radical grafting from polymerization. But also examples related to grafting onto or grafting through are reported as well as functionalization by physical adsorption using layer-by-layer assembly from the beginning.[31–33] In the following we briefly discuss a few selected studies and early examples of charge-based gating.

One of the first examples of gated nanopores reported in 1995 from Martin and colleagues referring to metal nanotubes showing permselective ion transport controlled by applied potential which have an analogous performance to that of commercially available polymers.[34] Early examples on gating in ceramic nanopores presented by White *et al.* in 2006 were based on modification of glass nanopore electrodes demonstrating pH-dependent ion selectivity based on electrostatic forces at the pore orifice.[35] Interestingly in this example different chemical functionalities were introduced at the exterior and interior surfaces of the pore (–CN and $–NH_2$ terminal groups, respectively).

In a follow-up work, the author reported on photo-induced molecular transport by functionalizing spiropyran in the single pore orifice, which could be switched between ''on'' and ''off'' states through conversion between the neutral surface-attached spiropyran and the more polar merocyanin form.[36] Although merocyanine is often sketched as a zwitterion it has to be considered that different conformers exist[37,38] and transformation from spiropyran to merocyanine is usually far from one hundred percent conversion.[39] Therefore, spiropyran homopolymer grafting has been attempted. Spiropyran has been grafted from silica mesopores as a homopolymer in a surface-initiated ring opening metathesis polymerization (SI-ROMP).[39] Additionally, the photo-responsive behavior of the homopolymers was systematically investigated using NMR spectroscopy in this study.[39] Furthermore, spiropyran in combination with PEG has been grafted to ion track etched nanopores.[40] In an early work from Li and Ito, surface charge, and with this the ionic pore accessibility of cylindrical polystyrene-poly(methylmethacrylate) diblock copolymer (PS-*b*-PMMA) nanopores, was adjusted using 1-ethyl-3-(3-dimethylaminopropyl)carbodiimide (EDC) and grafting of tetraethylene glycol monoamine ($(PEO)_4NH_2$) resulting into amidation of the surface carboxyl groups.[41] Besides the polymer response to stimuli in 2005, the first indications of polymer-solvent interaction for gating nanochannels have been obtained based on Molecular Dynamics (MD) simulations.[42] Following these early examples, nanopore gating is now systematically realized by functionalization with responsive polymers. Starting between 2006 and 2009, the first pH-responsive grafted polymers such as polyacrylamide,[43] poly(2-(dimethylamino)ethyl methacrylate) (PDMAEMA),[44] temperature responsive poly(*N*-isopropylacrylaminde (PNIPAAM)) in opal nanopores[45] and the zwitterionic poly(methacryoyl-L-lysine) brushes in a single conical etched ion track nanopore were used.[46] Zwitterionic polymers are especially interesting as they result in so-called bipolar pores blocking ion accessibility independently of their charge.[47–50] Azzaroni *et al.*[51] reported in 2009 the integration of poly(4-vinyl pyridine) (P4VP) brushes as pH-responsive polymers in the inner walls of single nanochannels enabling transport to be controlled by changing the proton concentration. Even beyond pH, basically all available stimuli from temperature responsive gating,[45] ion- or ligand-responsive gating,[52] light-induced,[36,53] to redox responsive gating[54] and even magnetic gating[55] have been demonstrated (Fig. 1a–f). For example, Ensinger and colleagues as well as Azzaroni and colleagues demonstrated optical gating of nanofluidic devices using a photo-cleavable group to demonstrate ionic permselective transport through the channels.[54] Although this photocleavage is not reversible, this strategy is especially interesting to induce significant changes in composition of pore wall surface and polarity/wettability which cannot be reached just by light-induced conformational changes such as those observed for spiropyran or other photo-responsive molecules. An example for redox-responsive gating in polymer-functionalized nanopores has been demonstrated upon functionalization of mesoporous silica films with polyvinylferrocene (PVFc) and poly(2-(methacryloyloxy)ethyl ferrocene carboxylate) (PFcMA) in a grafting from and a grafting through approach, respectively.[54] It has to be noted that gating was still achieved by chemical oxidation and reduction which is a slow process as the mesoporous matrix was non-conductive. Nevertheless, this study not only demonstrates the redox-responsive ionic mesopore accessibility but also provides a comparison between grafting onto and grafting from approaches and gives first insights into the influence of wettability on ionic pore accessibility gating. The significant changes in wettability upon oxidation of these polymers have been demonstrated on planar surfaces for these polymers.[56]

Besides responsive homopolymers statistical copolymers and block-copolymers have been also grafted to nanopores, for example, allowing the use of multiple stimuli for gating, and allowing to understand the influence of chain architecture on gating. For example, Zhu and colleagues demonstrated a temperature and pH-responsive nanopore after grafting from of a statistical copolymer consisting of PNIPAA and poly(acrylic acid) (PAA) using a free radical polymerization in a conical ion track etched nanopore.[57] Besides combining two responsive monomers, examples on multi-responsive homopolymer functionalized nanopores exist for example using poly(2-(methacryloxy)ethyl phosphate) (PMEP) in combination with pH and two valent ions such as calcium or magnesium.[52] Recently our own group demonstrated the re-initiation of a controlled photoiniferter-initiated polymerization allowing a mesoporous silica film to be functionalized with DMAEMA-*b*-MEP. The PDMAEMA-*b*-PMEP functionalized mesoporous silica film was demonstrated to gate from an anion selective to a cation selective nanopore while adjusting the pH from acidic to basic.[58] Interestingly, at intermediate pH no zwitterionic bipolar nanopore was observed indicating the influence of chain architecture on the resulting nanopore transport. Besides pH, ions such as calcium ions modulate the transport in these nanopores. Jiang and co-worker introduced a self-assembled block copolymer/homopolymer (PS22k-*b*-P4VP17k/hPS4k blend polymers) in asymmetric polyethylene terephthalate (PET)

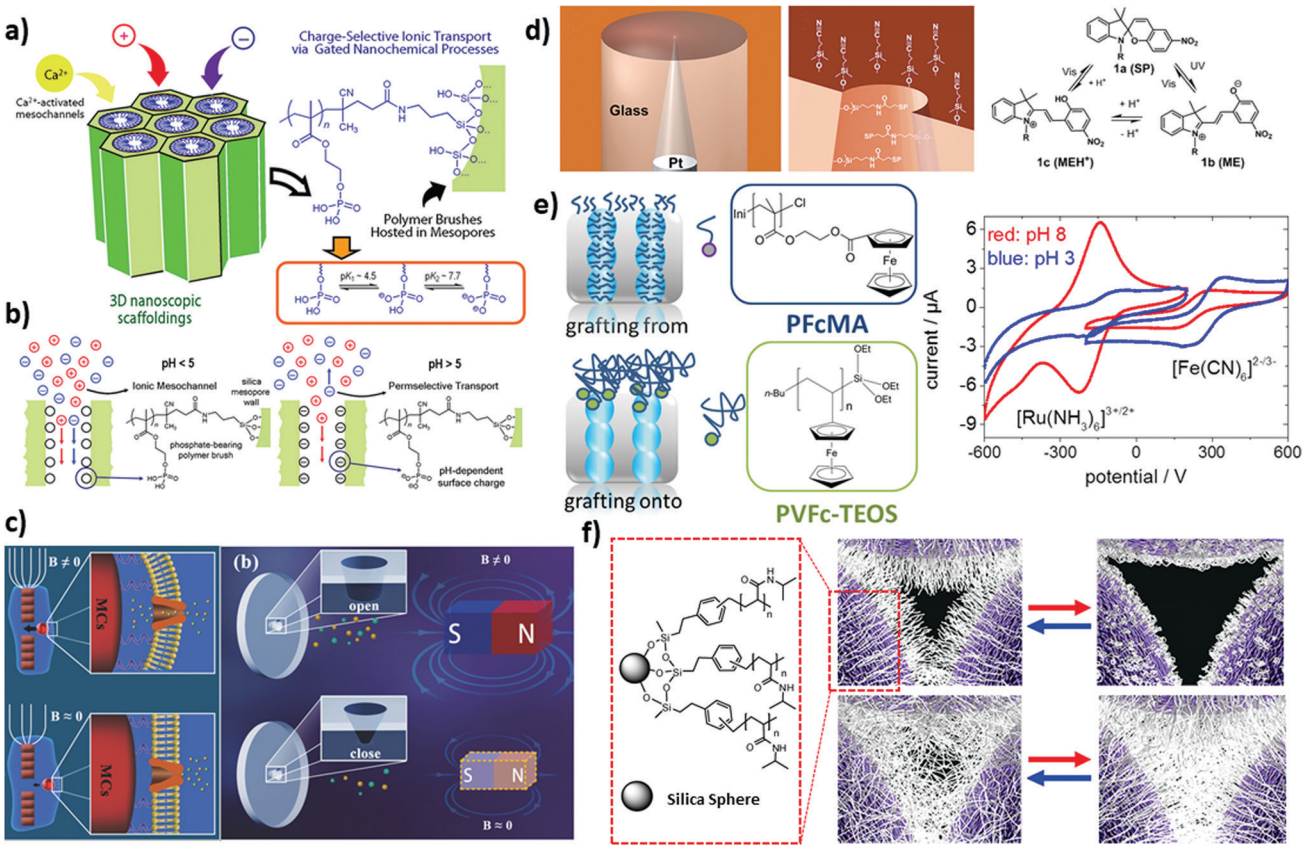

Fig. 1 (a) Schematic illustration of mesostructured polymer–inorganic assembly with phosphate-bearing polymer brushes. (b) The corresponding ionic transport process at different pH values: pH < 5, no exclusion of ionic species, pH > 5, permselective transport of cations, reprinted with permission from ref. 52 Copyright (2012), American Chemical Society. (c) Schematic depiction of a homing pigeon-inspired nanochannel modulated using a magnetic field in order to control the ionic current, rectifying ability and conductance through elastic deformation of the nanochannel, reprinted with permission from ref. 55 Copyright (2018). John Wiley and Sons. (d) Reversible transformation of the spiropyran molecule between neutral and positively charged forms over irradiation of different wavelengths along with a schematic representation of a glass nanopore electrode (selectively modified at the interior and exterior surfaces with spiropyran and cyanopropyl groups, respectively) acting as a photoswitching reversible gate. Reprinted with permission from ref. 36 Copyright (2006), American Chemical Society. (e) Schematic illustration of redox-responsive mesoporous membrane silica thin films functionalized with ferrocene-containing polymers, (top left) polyvinylferrocene (PVFc) and (bottom) poly(2-(methacryloyloxy)ethyl ferrocene carboxylate) (PFcMA), by using either a grafting to, or a grafting from approach. (right) Cyclic voltammograms for the initiator modified pore surface at pH 3 (grey triangles) and pH 8 (black circles) for a positively ($Ru(NH_3)_6^{3+}$, −0.6 to 0.2 V) and negatively charged ($Fe(CN_6)^{3-}$, −0.2 to 0.6 V) probe molecule. Reprinted with permission from ref. 54 Copyright (2013), John Wiley and Sons. (f) Schematic depiction of a temperature-responsive colloidal nanopore modified with thin (15 min polymerization) and thick (90 min polymerization) poly(N-isopropylacrylamide) brushes (exhibited positive and negative gating behaviour with temperature changes, respectively). Reprinted with permission from ref. 45 Copyright (2007), American Chemical Society.

bullet-shaped nanochannels which showed selective, pH-gated ionic transport behaviour resulting from the wettability and the pH-actuated changes in the surface charge.[59] In another recent study by Guangyan *et al.* polyethylenimine-*g*-phenylguanidine (PEI-PG, polymer bearing rich guanidinium groups) modified nanochannels were presented for specific recognition of phosphorylated peptide (PP) in a biosample. The sensing mechanism was based on strong interaction of guanidinium groups with PP leading to shrinkage of the grafted polymer in the channels and the corresponding ''off–on'' change of the ion flux.[60]

Using charge and charge density for nanopore transport control and gating it has to be considered that the spatial confinement influences charge regulation. This might not be detrimental in cases where only extreme basic and acidic pH-values are compared but it will be increasingly detrimental for small pH-changes or pH-sensitive applications. Confinement refers to the reduced space for polymers in nanopores with respect to the equilibrium space occupied by a polymer chain in solution. This limitation in available space with respect to the required space induces a shift in the equilibrium state of the polymer chain, for example, affecting charge regulation as the polymer chain tries to optimize entropic and enthalpic contributions while not being able to increase distance between charges as possible in solution. These effects of confinement on charge regulation are commonly indirectly detected, *e.g.* using cyclic voltammetry for ionic transport detection of redox-active model ions (Fig. 2a). Especially confinement-controlled charge regulation of polymer filled pores has been theoretically and experimentally demonstrated by Azzaroni and Szleifer (Fig. 2b)

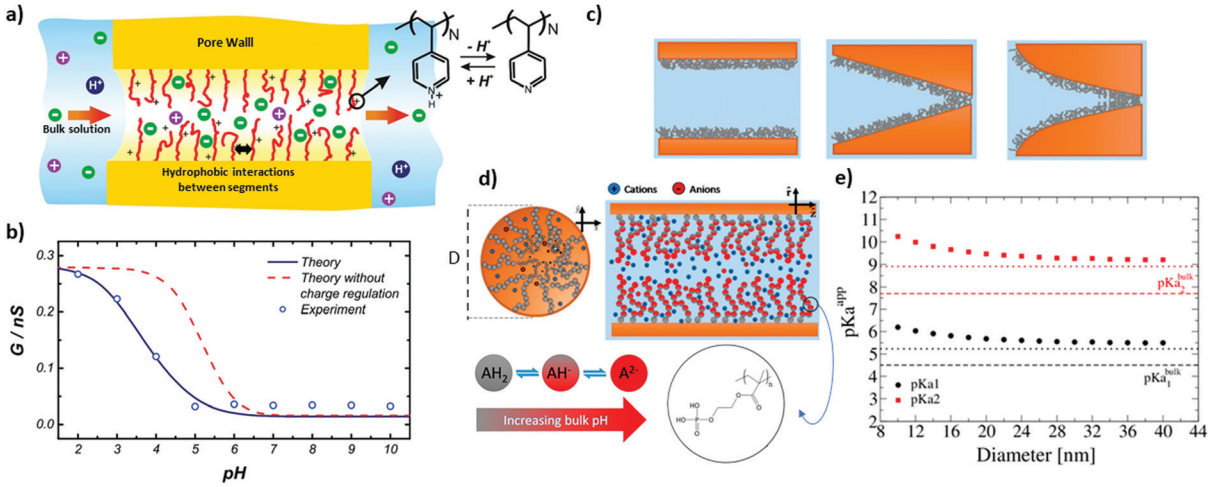

Fig. 2 (a) Schematic illustration of a poly (4-vinyl pyridine) modified cylindrical nanochannel along with (b) the experimental conductance values of the single nanochannel as well as the theoretical predictions as a function of the environmental pH values. Reprinted with permission from ref. 15 Copyright (2010), American Chemical Society. (c) Schematic depiction of (from left to right) cylindrical, conical, and trumpet-shaped nanochannels modified on the inner walls by poly(2-(methacryloyloxy)ethyl-phosphate) (PMEP), along with (d) the corresponding section of the modified cylindrical nanochannel as well as three chemical states of PMEP ($PMEPH_2$ (AH_2), $PMEPH^-$ (AH^-), and $PMEP^{2-}$ (A^{2-})). (e) Predicted apparent pK_a as a function of cylindrical nanochannel diameter (horizontal dashed lines and dotted lines show the pK_a values of the bulk and the predictions based on the simple analytical model, respectively). Reprinted with permission from ref. 61 Copyright (2016), American Chemical Society.

using cyclic voltammetry to generate experimental titration curves.[15] Azzaroni, Szleifer and colleagues investigated the solution pH dependent ion transport through a nanochannel with a diameter below 10 nm functionalized with 4-polyvinylpyridine (4-PVP) and observed a shift of more than one pH–unit together with a broader transition between the pK_a value detected for 4-PVP in the nanochannel *versus* the one in solution. Based on the molecular theory from Szleifer and coworkers this was attributed to the spatial confinement forcing charges to stay within a small distance from each other. According to this study, the polyelectrolyte functionalized nanopore can equilibrate towards the uncharged state ascribing to the charge regulation mechanism in order to minimize the electrostatic repulsions in the system. From the numerous modeling studies on polymer functionalized nanopores and confinement effects on charge regulation and ligand binding we would like to highlight that in 2016, Szleifer *et al.* extended these insights by theoretically investigating PMEP functionalized nanopores (Fig. 2c–e).[61] Their results demonstrate a strong shift of both pK_a values by around one pH unit. Our research group experimentally observed a consistent pK_a shift for PMEP modified mesoporous silica films for the first pK_a value whereas the second pK_a value could not be detected anymore under the applied experimental conditions.[62] In 2008, Ivory and colleagues proposed a pH-shift within the Debye Screening Layer close to the pore wall of nanochannels using the pH-responsive ratiometric dye SNARF-1® as the optical sensor.[63] A similar observation was presented by Yamaguchi *et al.* analyzing amine-functionalized silica pores with a diameter below 5 nm using different dye pH-reporter molecules.[64] Using dye-reporter molecules is an interesting approach to detect charge regulation. In particular, SNARF-1® is frequently used in pH-change detection of cells down to single molecule detection.[65] Adapting this strategy to nanopores in the first place would profit from a broader dye-reporter library as the relevant pH-range is not limited to physiological pH but covers the entire pH-range. In this context for example a novel ratiometric thiazol-based dye (amide (4-(5-methoxy-2-(pyridin-4-yl)thiazol-4-yl)-*N*-propylbenzamide)) has been reported as a dye-reporter molecule covering the pH range from 1.5 to 5.[66] Although an inspiring approach, it has to be taken into account that the dyes themselves might influence the charge situation and thus the pK_a value. Consequently, the system has to be well-designed. The mentioned pK_a shifts and changes in shape of the titration curve is of relevance in different applications from sensing, separation, to enzyme stabilization and release. Kleitz and colleagues demonstrated that charged drugs incorporated into pH-responsive protein modified MCM-48 mesoporous nanoparticles (MSN) influence the stability and pH-responsive release.[67] They proposed using synergistic effects of *e.g.* pH-responsive protein and MSNs to pave the way toward efficient oral (nano) formulation of therapeutic agents.

Besides charge regulation and charged based gating, hydrophobicity or wettability strongly determines the interaction of nanoporous materials with fluids, in most cases water, as well as with molecules of varying polarity.[68–72] Bringing nanoscale pores in contact with liquid water, the water can either imbibe into the nanopores or be excluded comparable to a Cassie-like wetting state. The wetting state is reported to be determined by nanopore characteristics such as the pore diameter and pore wettability, and the pore opening angle in the case of inverse opal monolayers.[73–77] Gating or switching between water exclusion and water imbibition has been demonstrated for porous materials. Ran *et al.* reported the influence of the surface structure of nanoporous alumina inducing a transition from the Cassie to Wenzel wetting state.[78] Siwy and colleagues used

electric field induced wetting and dewetting to reversibly gate between water imbibition and water exclusion.[79] It has to be noted that relatively high voltages are necessary to achieve water evaporation and thus voltage-driven water removal from nanopores. Further voltage gating in SiN pores[80] and in porous gold has been demonstrated.[81] In the majority of studies a transition contact angle of 90° is stated for water exclusion to water imbibition. Work from Berg[82] and Vogler[83] states a transition contact angle of 65° looking at hydrophobic forces and the molecular scale which is picked up by work on nanopores from Jiang *et al.*[72,84] It has to be noted that reporting advancing and receding contact angles is important for being able to compare different experiments. In a systematic study by Samuel *et al.* advancing and receding contact angles were regarded to be the only meaningful measurements (as opposed to static water contact angle, contact angle hysteresis and sliding angle) to correlate with wetting and adhesion forces, respectively.[85] The role of contact angle hysteresis for porous material wetting[86] as well as for inhomogeneous porous materials is considered by Herminghaus and colleagues.[87,88] Furthermore, a theoretical study from Luzar and colleagues points to the complex interplay of charges and wettability.[89] One interesting aspect of wettability in porous materials is the possibility to adjust the contact angle at which the wetting transition from the Cassie to Wenzel state and thus from water exclusion to water imbibition occurs which has been especially investigated for inverse colloidal monolayers. Silica inverse colloidal monolayers show a transition contact angle for water imbibition between 20°–50° while being tunable by material characteristics such as the pore opening angle and the applied solvent.[73,90–92] The transition contact angle for fluid imbibition thereby depends on the angle between the pore neck and the tangent to the pore wall. Knowing the transition contact angle at which fluid imbibition occurs, gating from water exclusion to water imbibition, using stimuli-induced molecular changes, can be achieved, and even used for sensor concepts,[92,93] for example. Stimuli-induced conformational changes, as for example the transformation of spiropyran to merocyanine are known to induce relatively small changes in polarity with contact angle changes at planar surfaces of around 10°–15°.[37] Nevertheless, such molecular conformational changes can be used to trigger water imbibition into nanopores in case the initial contact angle is positioned only slightly above the transition contact angle. It should be noted that in the case of surfaces with nanoscale roughness, larger contact angle changes can be expected at well-defined surface energies and wetting transitions.[94] This transition from water exclusion to water imbibition has been triggered by stimuli such as pH,[75] voltage as mentioned above,[79] or light-induced polarity change of spiropyrans[95] or azobenzenes.[94] Larger contact angle changes at structured or porous surfaces, and thus water exclusion to water imbibition transitions starting at a higher contact angle difference from the transition contact angle, can be achieved when unipolar molecular parts are removed. One example for this approach is represented by using light-induced removal of photo-sensitive protection groups. Another example is conical ion track etched nanopores functionalized with photo-responsive azobenzene units known to interact with beta-cyclodextrin in their *trans* isomer state which has been demonstrated to show light based wettability gating.[96] Upon visible light irradiation the azobenzene molecules at the pore wall switch from the *cis* to their *trans* isomer (Fig. 3a and b). As the *trans* isomer interacts with the beta-cyclodextrin the pore wettability changes from hydrophobic to hydrophilic after beta-cyclodextrin binding. This change is reversible upon UV-irradiation.[96]

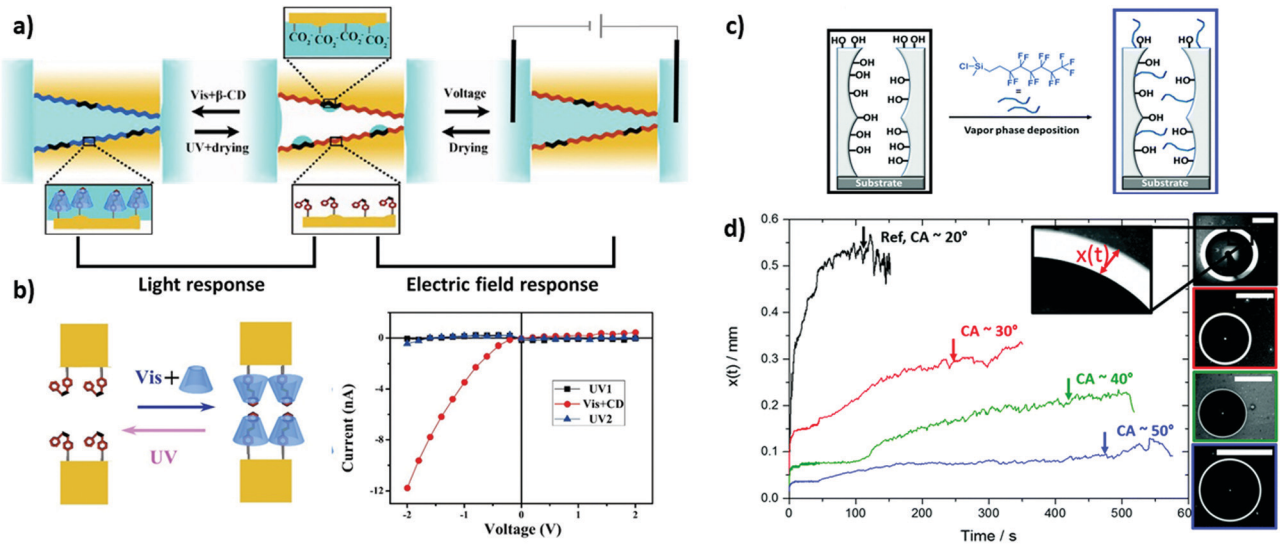

Fig. 3 (a) Schematic representation of Azo-modified nanochannels with controlled wettability by light and electric field. (b) Schematic depiction of the light-driven reversible reaction between the azobenzene derivative and β-cyclodextrins in the nanochannels along with the corresponding *I*–*V* characterization of the reaction, reprinted with permission from ref. 96 Copyright (2018), American Chemical Society. Schematic illustration of (c) mesoporous silica films functionalized by vapor phase deposition of 1*H*,1*H*,2*H*,2*H*-perfluorooctyl dimethylchlorosilane (PFODMCS) along with (d) the imbibition ring ($x(t)$) as a function of time (scale bar = 2 mm), reprinted with permission from ref. 115 Copyright (2020), Royal Society of Chemistry.

In case water imbibes into the nanopores the observed phenomena depend, for example, on the pore size. For very small pores (<1–2 nm) such as graphene nanopores, no bulk behavior for water is observed anymore and high transport rates have been reported especially in the case of hydrophobic nanopores of this size.[97–104] This increase in water transport rates is known in biological pores like aquaporin.[10] Furthermore, an interesting phenomenon of hydrophobic nanoscale pores is hydrophobic gating due to water evaporation.[68,105] MD simulation states that pores with a diameter below 2 nm are able to show hydrophobic gating.[105–108] Experimental studies observe ion rectification explained by hydrophobic gating even for larger asymmetric pores.[79,109] These observations clearly demonstrate the importance of wettability design for nanopore transport.

In case water imbibes into nanopores with a diameter larger than one to two nanometers, the critical infiltration pressure is often given by the Laplace equation and the macroscopically observed imbibition speed has been reported to macroscopically follow the Lucas Washburn or Darcy law in case evaporation is excluded.[81,110,111] In thin mesoporous films evaporation cannot be neglected and evaporation and condensation at the fluid front have to be considered to describe fluid behavior and fluid imbibition.[112] When depositing a water droplet onto such a mesoporous film, a fluid imbibition ring around this droplet becomes visible. Different studies report the width and imbibition speed of this imbibition ring which can be correlated to the mesoporous structure[113,114] and wettability[75,115] (Fig. 3d). Furthermore, the fluid front of this kind of imbibition zone around a water droplet oscillates indicating constant evaporation condensation cycles at ambient conditions.[77,116] Deviations in the imbibition behavior from the Lucas Washburn or Darcy's law are usually related to evaporation and eventually capillary condensation. This capillary condensation is an interesting feature of nanoscale pores as they can be filled with fluid even when only in contact with vapor.[70] Thereby, water capillary condensation is usually described using the Kelvin equation. The Kelvin equation is even used for characterization of water adsorption in mesoporous thin films using environmental ellipsometry.[117] During characterization often the macroscopic apparent contact angle is used which strongly determines the obtained results. Sorption dynamics might be relevant and structure dependent,[114,118] and the solvent used of course plays a role,[119–121] without going into details here. Interestingly, Grosso and colleagues used the Kelvin equation to deduce an effective nanoscopic contact angle and compared this contact angle with the macroscopically measured one using hydrophobized mesoporous silica films. They observed comparable values for this nanoscopic contact angle deduced from the Kelvin equation with the advancing macroscopic contact angle on these mesoporous films.[121]

Beyond fluid imbibition, evaporation, and condensation the nanopore wettability seems to affect the molecular transport.[59,122] Walcarius and colleagues investigated the influence of silanes with varying nonpolar chain length grafted onto ceramic mesoporous films on mass transport using cyclic voltammetry.[123] Adjusting wettability in mesoporous silica films using varying amounts of 1*H*,1*H*,2*H*,2*H*-perfluorooctyldimethylchlorosilane (PFODMCS) showed the influence of this functionalization, and the corresponding gradual increase in contact angle on ionic pore accessibility (Fig. 3c and d).[115] The obtained data on molecular transport and water condensation indicate that close to the transition contact angle the transport becomes pH-dependent and can occur through a condensed water layer along the pore walls.[75] Using impedance spectroscopy a reduced diffusion coefficient with increasing wettability was observed.[95] Interestingly, the wettability of polyelectrolyte modified surfaces[124] and nanoporous surfaces[125] can be influenced by exclusively replacing the counterion of the polyelectrolyte, thereby strongly influencing the pore accessibility of other ions, demonstrating the interplay of ligand binding and wettability in polyelectrolyte functionalized nanopores.

Recently, the correlation between nanopore structure, functionalization and water wettability, imbibition, and evaporation was applied for example to serve as a readout mechanism for local temperature changes in porous materials induced by local plasmonic heating.[126] Another recent example of using this correlation is the observation that water droplets on porous surfaces dilute upon evaporation.[127]

In addition to electrostatic interactions and wettability, ligand binding or specific interactions with functional groups at the nanopore wall strongly influence the molecular passage or adsorption of dissolved molecules through the nanopore. In the context of nanopore ion transport two main mechanisms are discussed governing selective ion transport. In case the pore size is in the range of the dimensions of the hydrated ions, and this is the case for many biological selectivity centers *e.g.* in the potassium channel,[8] the driving force for transport is the energy needed for dehydration of the ions. Regarding technological materials, graphene, for example, represents this transport mechanism while most of the above mentioned materials do not reach this pore size in the micropore range according to the IUPAC definition.[128] In case the pore size is larger, as for most mesoporous materials or solid state nanopores, ligand binding or binding affinity strongly determines the transport characteristics. Inspired by biological pores showing transport selectivity, protein, and polymer brushes based nanopores have emerged with potential to achieve such specific binding interactions and selective transport. Siwy *et al.*[129] demonstrated a protein biosensing system based on conical gold nanotubes embedded within a robust polymeric membrane and functionalized with a bio-recognition agent including streptavidin, protein-G and antibody. Unlike the previously reported stochastic systems,[130,131] the blockage of the ion current by binding the protein analytes was used instead of analyzing transient current pulses. In another example reported by Azzaroni *et al.* a bio recognition process was incorporated inside a single conical nanochannel through simple electrostatic assembly of bifunctional, multivalent ligands on a charged pore wall. The nanochannel showed good bio-specific features as well as non-fouling properties toward unspecific proteins.[33] Dahlin *et al.*[13] showed a functionalized nanopore with poly(ethylene glycol) brushes, which

fully blocks the translocation of proteins, can be reversibly gated to an "open" state by binding of single IgG antibodies that disrupt the entropic barrier presented by the polymer brush. Apart from experimental works, a theoretical study reported by Tagliazucchi and Szleifer in 2015 gives interesting insights into the protein ligand-receptor binding equilibrium in nanoscale pores and confinement.[132] For example an optimum binding amount at intermediate grafting density as well as an optimum linker length is reported. Interestingly, the optimum linker length depends on the pore size as the optimum situation prefers placing proteins close to the channel center resulting in a maximum volume fraction of the bound protein in the nanopore. This is especially of importance for protein pore blocking and in the context of sensing or biomolecule stabilization and biocatalysis. Especially when charged proteins are used the nanochannel conduction might be strongly influenced by the protein location along the nanochannel cross section either reducing or increasing nanochannel conduction which is based on an interplay of volume exclusion and surface charge effects.

Gradual nanopore accessibility *via* polymer functionalization control

To go beyond gating and towards gradually adjusted nanopore transport, a gradually tunable polymer amount, and with this *e.g.* gradual adjustment of charge density has to be experimentally realized. Furthermore, polymer chain composition in nanoscale pores as well as multifunctional nanopores represent an experimental step towards gradually adjusted nanopore accessibility. An essential step towards this goal is the application of controlled polymerization techniques to nanoscale porous materials. Grafting density, chain length and thus polymer amount, for example, encode charge density. Thus they not only affect molecular transport but are important parameters in polymer modified porous materials also affecting ion and polymer density distribution along the pore cross section[14,133,134] or protein adsorption.[135] The majority of controlled polymerizations in nanoscale pores is based on radical polymerization such as surface-initiated atom transfer radical polymerization (SI-ATRP), surface-initiated reversible addition–fragmentation chain-transfer (SI-RAFT), or iniferter-initiated polymerizations, although examples on other polymerization techniques such as SI-Nitroxide-Mediated Polymerization (SI-NMP), SI-ROMP or ionic polymerization have been reported.[136–138] Regarding ATRP for example, the functionalization of porous nanoparticles with PDMAEMA was reported.[136,139] This study demonstrated low dispersity ($Đ < 1.08$) in 10–15 nm cylindrical mesopores upon adding Cu(II) halide as the deactivator to the reaction mixture. Although controlled ATRP was observed, Charleux and co-workers also pointed towards irreversible termination inside the mesopores upon ATRP grafting from polymerization in mesoporous silica particles.[140] Recently, variations of ATRP such as ARGET-ATRP in mesopores have been demonstrated,[141] and the confinement influence was further analyzed. For example, the group of Schönherr further investigated the curvature and pore size influences on SI-ATRP using anodic alumina nanopores with high aspect ratios.[142] Their study demonstrates a curvature and pore diameter effect on the polymerization kinetics and confirms the control of pore filling by using SI-ATRP. For highly confined samples (19 nm pore radius) all the monomers initially present inside the pore were converted to PDEGMA chains with an accelerating rate attributed to chain stretching and confinement. With increasing pore diameter the confinement became less important with a transition to similar polymerization kinetics as compared to planar surfaces for 65 nm or larger radius pores. It has to be noted that the pore radius for nanopores applied to transport control is often still significantly smaller than 19 nm. Regarding SI-RAFT and iniferter-initiated polymerizations Chen *et al.*[143,144] applied light induced SI-RAFT to graft zwitterionic and thermoresponsive monomers on silica nanoparticles in the presence of oxygen. Re-initiation of polymerization and high pore filling degrees were obtained by Tom *et al.* By grafting chloroprene to silica nanoparticles using SI-RAFT, Zheng *et al.*[145] demonstrated that even on particle surfaces SI-RAFT of chloroprene is slower than free RAFT polymerization.[146] Besides radical controlled polymerization a few examples on SI-ROMP as well as on anionic polymerizations on surfaces and in porous materials have been reported: anionic polymerization lacks control when applied to surfaces such as silica as residual water is almost always present and disturbs polymerization, resulting in inhomogeneous polymerization and relatively large $Đ$. Nevertheless, polymer layers with a $Đ < 1.21$ have been obtained on silica nanoparticles after systematic optimization of the reaction conditions.[147,148] For SI-ROMP two approaches can be considered. Either designing a ROMP catalyst carrying an anchor group allowing surface binding[149] or modifying the surface with double bonds to coordinate the catalyst followed by ROM polymerization in the presence of a suitable monomer. The second approach is more frequently used in the context of SI-ROMP. The group of Buchmeiser demonstrated metathesis graft polymerization in the context of porous materials for chromatography.[150–152] Zhou and colleagues combined ATRP and ROMP for asymmetric polymer functionalization discriminating both sides of an anodic aluminium oxide porous material.[153] Our research group successfully applied SI-ROMP to generate photoresponsive spiropyran and spirooxazine homopolymers in silica mesopores which cannot be synthesized as a homopolymer in larger molecular weight using radical polymerization.[39]

Despite the numerous developments in polymerization control in nanoscale pores relatively few studies directly correlate the insights into controlled polymerization in such pores with the experimentally resulting transport properties. On the other hand, theoretical studies demonstrate the influence of polymer amount and charge density, polymer sequence, molecular weight, or polymer distribution on ionic transport, highlighting the relevance of polymerization control in nanopores.[14,135,154–158] Experimentally, it has been demonstrated that polymer amount, and with this charge density in nanopores, and consequently ionic permselectivity can be gradually adjusted using different

polymerization reactions such as ATRP, RAFT, and iniferter-initiated reactions.[137] Clochard and colleagues adjusted the PAA filling degree of PVDF ion track etched pores with pore diameters below 50 nm.[159] This study systematically analyzes polymer filling by combining different characterization techniques such as atomic force microscopy (AFM), infrared spectroscopy (IR), X-ray photoelectron spectroscopy (XPS), and demonstrates the influence of pore filling on size exclusion and Pb^{2+} ion sensitivity. In 2015 we reported the correlation of pore filling control using free-radical polymerization in mesoporous silica thin films with pore diameters below 10 nm in combination with a strong polyelectrolyte PMETAC showing gradual increase in anion pore accessibility with increasing polyelectrolyte density (Fig. 4a–c).[134] The same effect but with pH-dependence was observed by using iniferter-initiated polymerization in similar mesoporous silica films grafting pH-responsive zwitterionic polycarboxybetaine methyl acrylate (PCBMA) polymer chains from the pore wall.[160] Besides ATRP and free-radical polymerization this iniferter-initiated polymerization appears to be a suitable polymerization technique to functionalize small mesopores in a controlled manner. Using this approach re-initiation of the polymerization and with this block polymer chain sequence generation in mesopores with pore diameters below 10 nm has been demonstrated.[58,145] Experimentally combining PDMAEMA and 2-(methacryloyloxy)ethyl phosphate (MEP) into a block copolymer allowed this pH-dependent positively and negatively charged pore to be compared to a zwitterionically functionalized pore. Interestingly, the chain architecture and thus charge distribution within nanopores seems to influence the transport. Zwitterionically functionalized pores using PCBMA show a polymer amount and thus charge density dependent ionic pore accessibility at acidic pH when PCBMA is positively charged. At basic pH and thus in their zwitterionic charge these pores show the so-called bipolar behavior and exclude ions.[46,161] This exclusion was not observed for PDMAEMA-*b*-PMEP block copolymers/block cooligomers even if the pH is adjusted such that both monomers are expected to be charged. This observation leads to the conclusion that the chain composition is of importance.[58] Huang and Szleifer theoretically demonstrated that polymer chain sequence-controlled mixing of nonpolar and pH-responsive monomers allows the design of orthogonally responsive gates regulating ion transport.[155] Recently, Szleifer and colleagues even demonstrated based on their non-equilibrium steady state molecular theory that a gradient in block ratio of an acidic and a basic monomer in a 42 nm long nanopore with 13 nm diameter would serve as an ion pump or pH-responsive filter.[154] Consequently, theoretical studies serve as inspiration for experimental nanopore functionalization and transport design.

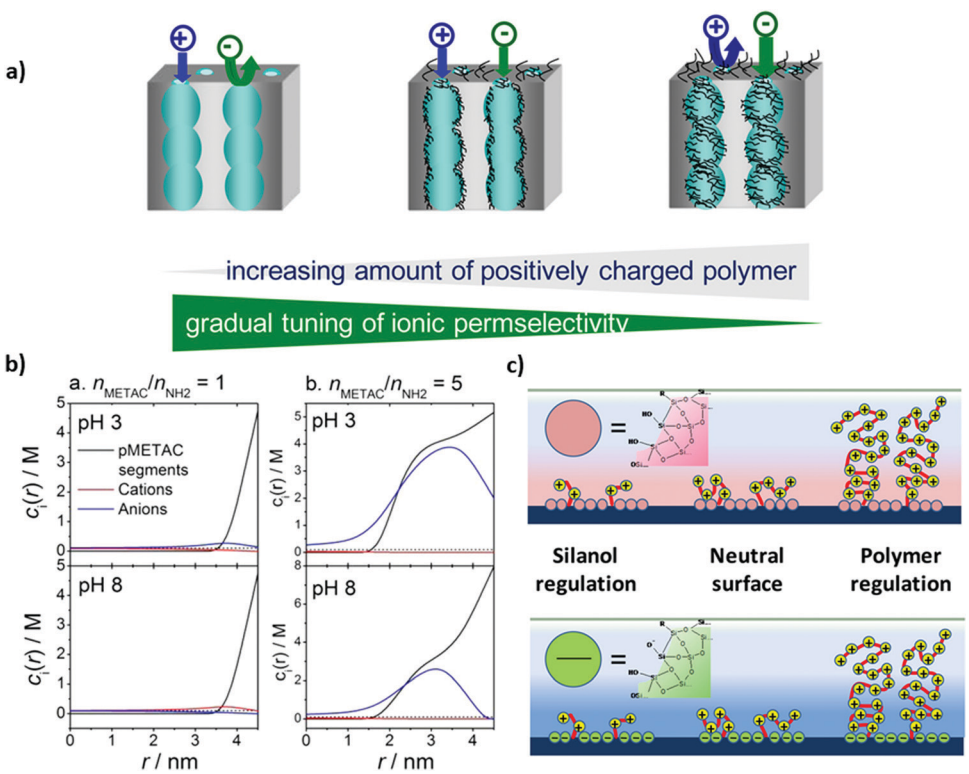

Fig. 4 (a) Schematic depiction of mesoporous silica thin films functionalized with PMETAC at various electrolyte density, (b) molar concentration of polymer segments, cations (K^+) and anions (Cl^-), as a function of the distance from the center of the pore, and (c) schematic depiction of the modified silica surface at acidic pH $<$ 3 (upper figure) and alkaline pH $>$ 7 (lower figure). Reprinted with permission from ref. 134 Copyright (2015), American Chemical Society.

Transport direction *via* asymmetric nanopore architecture

Beyond functionalization the nanopore architecture or the nanoporous material architecture design is of relevance for molecular transport control. This was demonstrated when ion rectification of conical ion track etched pores was discovered[162,163] demonstrating the benefit of asymmetry in transport direction concepts. In multipore nanoporous materials, such as mesoporous films, material architecture characteristics such as film thickness or multilayer arrangements are increasingly investigated. This resulted, for example, in Janus-type materials with side selective oil–water separation[164,165] or efficient osmotic energy conversion[166] due to asymmetric wettability or charge distribution. It also resulted in the fabrication of ultrathin porous films or layers to generate thin selectivity filtration centers.[167] Recent theoretical studies on nanopore asymmetry induced not only by asymmetric pore shape but also by asymmetric functionalization within the nanopore[154,155] indicate in which direction experimental nanopore functionalization has to develop.

Janus-type porous materials have demonstrated side selective oil water separation or have been discussed in the context of osmotic energy conversion. For example Jiang and colleagues demonstrated a ''water diode'' Janus membrane by combining a hydrophilic porous PET foil with a one side hydrophobic polytetrafluoroethylene (PTFE) layer.[164] Further functionalization rendered this Janus membrane magnetism or pH-responsivity. Side selective oil–water penetration through this membrane was demonstrated. A similar side-selective oil–water separation was demonstrated by Ikkala and colleagues[168] depositing a skin layer on a cotton support demonstrating directional water droplet gating. Using paper functionalized with silica gradients in low silica amounts, the silica coating leads to silica amount-dependent hydrophobization of the paper sheet. When applied in a material gradient side-selective hydrophobization and thus side selective oil–water separation was observed.[165] Different studies were looking at transport exclusively at the pore entrance or outer surface functionalized porous materials. For example Ma *et al.*[169] demonstrated pore-wall independent transport control using anodic aluminium oxide (AAO) locally functionalized with gold at the outer surface allowing subsequent selective further binding of functional molecules such as polymers or DNA to the gold. A similar approach was presented by Azzaroni and colleagues functionalizing mesoporous films exclusively at the outer surface with a few nanometers thick light-responsive polymer.[54] Changing from hydrophobic to hydrophilic upon irradiation while gating the pore wall and polymer charge upon pH-change a multi-stimuli-responsive nanoporous layer was obtained. Side selective functionalization was also achieved for ultrathin 1D porous materials. A comparable concept of combining hydrophobic rejection with electrostatic ion discrimination was reported by Su and colleagues.[170,171] A pH-responsive, ion discriminating mesoporous silica film with a hydrophobic polydimethylsiloxane (PDMS) layer in contact with the solution was used and cation selective transport was observed. Jiang and his group demonstrated a side selective functionalization of conical PET nanopores using an acid-driven PS-*b*-P4VP block copolymer assembled porous layer at the large pore opening and a base-driven PAA brush functionalized gate at the small pore opening creating a bioinspired heterogeneous ion pump membrane with a selective unidirectional ion pumping function for the anion.[172] The key step to this performance is the combination of asymmetric pore shape and precise, orthogonal gating function. Based on such an asymmetric design single channel ion pumps have been designed.[172–174] In the context of pore arrays, the functionalization of the pore entrance of a block-copolymer assembled porous layer with a high pore density of $\sim 10^{11}$ cm^{-2} capped by a layer of hyperbranched polyethyleneimine (PEI).[166] Due to the high channel density and its functionalization, ion selectivity and unidirectional ion transport were achieved resulting in the reported osmotic energy conversion output power of 22.4 W m^{-2} at a 500-fold salt gradient. Although this approach allows relatively large membrane area fabrication upscaling of nanopore based osmotic energy conversion is still controversly discussed, taking large scale application and its process parameters, such as ion concentration polarization, into account.[175,176] Wen and colleagues theoretically and experimentally investigated the optimization of ion transport through functionalized conical nanopores in the context of separation selectivity and osmotic energy conversion.[177] They reported that the ion selectivity as well as the energy conversion efficiency is effectively enhanced upon optimization of the local functional density translating into the local surface charge or by introducing a layer with dense surface charge at the low concentration side of the porous layer.[177] Beyond potential performance optimization, and without mentioning every single study in this field, these selected examples demonstrate that porous layer architecture design and layer-wise local functionalization allow separation and thus individual study, of the transport determining effects such as the influence of the outer surface or the inner pore wall functionalization. Inspired by the design of biological pores or channels,[8] design strategies towards nanoscale precise placement of functional responsive molecules or polymers inside nanopores are expected to advance transport performance with respect to transport direction, ion pumping, and selectivity even beyond the side selective transport direction. This requires symmetry breaking within each individual nanopore. One detrimental step towards symmetry breaking has been the directed ion transport in conically or in general asymmetrically shaped nanopores.[178–182] Transport direction even with homogeneous functionalization along the pore thereby results from the geometrically induced asymmetric electrostatic potential distribution along the nanopore.[162] In addition to the geometric asymmetry, functionalization has been asymmetrically designed. But examples of experimental realization of nanoscale local polymer placement inside nanopores remain scarce. To achieve asymmetric functionalization along nanopores the reaction has to be locally limited to the nanoscale inside a nanopore. This renders nanofabrication methods known from planar surfaces, such as techniques based on contact, *e.g.* a tip being in contact with a surface to deposit a

material (dip-pen lithography) or colloids as a mask (colloidal lithography),[183,184] useless. In the context of nanopores, in 2007 the group of Siwy and Vlassiouk fabricated a nanofluidic diode with a positively charged tip side and negatively charged base side of a conical nanochannel by using active ester chemistry to transform the carboxyl groups at the large pore opening side inside the conical pore to amino groups.[185] This resulted in ion rectification degrees of several hundreds. The same concept was applied to biosensing after locally modifying the small pore entrance with a monoclonal antibody.[186] Local functionalization was achieved by side selective contact with the reagent solution. This approach is well-established for side selective functionalization of ion track etched nanochannels and allows so-called diffusion limited (polymer) functionalization (DLP). In 2010 Hou *et al.* demonstrated the asymmetric functionalization of a double conical pore of 12 μm length using responsive polymers using DLP.[187] By side selective monomer contact one cone was functionalized with the temperature responsive PNIPAAm and the other cone with pH-responsive PAA resulting into a multi-responsive, double conical nanopore (Fig. 5a). In 2015 Jiang and his group demonstrated that in such double conical and asymmetrically polymer-functionalized pores, here using a PAA gate, the location of the smallest diameter between both cones significantly influences ion transport, too (Fig. 5b).[188] Therefore, the position of the transition from one to the other cone was gradually shifted from the channel end to the channel center. The nanochannels with the PAA gates on the small base sides exhibited very strong gating and rectification properties. When the PAA gates were located at the large pore opening the gating abilities and rectification effects of the nanochannels were weakened and even reversed. Jiang and colleagues attributed this gate-location-dependent enhancement and inversion of the ion gating and rectification to the cooperation and competition between asymmetric geometries and the gate-position-controlled asymmetric surface charge distributions of the nanochannels.[188] Jiang and his group further reported on the pore entrance localized functionalization of a cigar shaped 10 μm long and up to 150 nm pore center radius pore with the two different polymers PVP and PAA at both entrances.[189] This nanopore design with two orthogonally charged gates demonstrated ion pumping (Fig. 5c).

Although the majority of examples on locally functionalized nanopores is based on ion track etched nanochannels with a length of usually larger than ten micrometers, several attempts in other materials exist. For example, Zhou and coworkers functionalized an AAO membrane using ATRP, dopamine self-polymerization (DOP-SP) and ROMP.[153] As the membrane was in contact with two different polymerization solutions at each side of the membrane asymmetric polymer functionalization

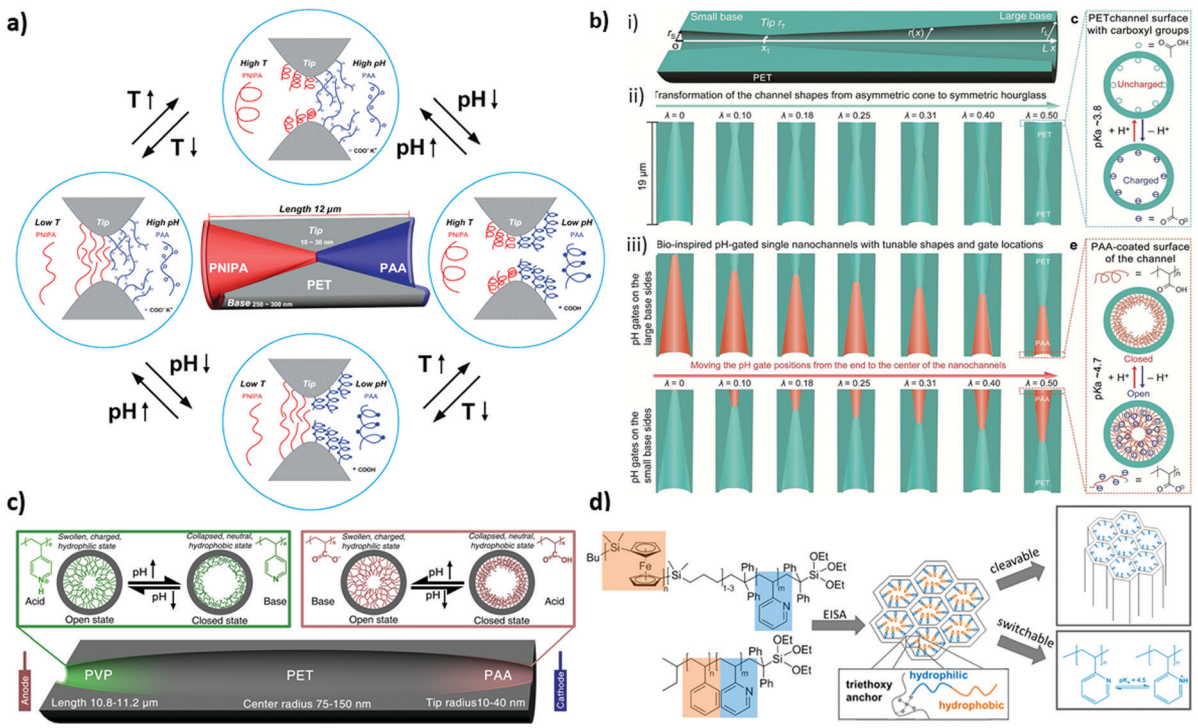

Fig. 5 (a) Schematic representation of an asymmetric dual responsive single nanochannel system locally modified by PNIPA and PAA on different sides of the inner surface of the nanochannel. Reprinted with permission from ref. 187 Copyright (2010), American Chemical Society. (b) Schematic depiction of an artificial single-nanochannel system and the corresponding geometry parameters and the pH-responsive conformational changes of the inner surface. Reprinted with permission from ref. 188 Copyright (2015), American Chemical Society. (c) Schematic illustration of the cross-section of a bioinspired single ion pump system based on the double-gate nanochannel and the pH-responsive conformation changes from the open to the closed state. Reprinted with permission from ref. 189 Copyright (2013), American Chemical Society. (d) Schematic of the in-situ-functionalization of a mesoporous silica film *via* evaporation-induced self-assembly of PS-*b*-P2VP-Si(OEt)$_3$ and PFS-*b*-P2VP-Si(OEt)$_3$ resulting in ionic permselectivity and pH-responsive transport properties. Reprinted with permission from ref. 196 Copyright (2020), Royal Society of Chemistry.

was obtained. Similarly double hydrophilic poly(3-sulfopropyl methacrylate potassium salt)@poly(2- (methacryloyloxy)ethyl-methylammonium chloride) (PSPMA@PMETAC), temperature and pH double responsive poly(*N*-isopropylacrylamide)@DMAEMA (PNIPAM@PDMAEMA), and hydrophilic/hydrophobic poly(3-sulfopropyl methacrylate potassium salt)@poly(hydrophobic pentadecafluorooctyl-5-norbornene-2-carboxylate) (PSPMA@PNCA-F15) polymer brushes-modified asymmetrical AAO membranes were reported.[153] Voelcker and co-workers reported functionalized AAO membranes with a series of anodization and silanization cycles. Following this strategy multilayered surface functionalities with silanes inside the pore channels are achieved which influence the wettability and transport properties of the membrane.[190] Using sol–gel chemistry and co-condensation our research group demonstrated that layer selective pre-functionalization of a multilayer mesoporous film can be used to localize subsequent initiator binding and the following polymerization to a specific layer in a multilayer mesoporous silica film.[191] Together with mesoporous film fabrication, using *e.g.* gravure printing, allowing down to approximately 15 nm thick homogeneous mesoporous film deposition a nanoscale step gradient was achieved.[192] Another approach toward nanoscale step gradient formation is accessible for ceramic mesopores fabricated by sol–gel chemistry using block-copolymer assembly for mesopore formation followed by polymer removal upon calcination or chemical extraction. Usually these mesoporous layers are deposited using dip-coating. Alternatives are spray or spin coating, for example. Using dip-coating the layer thickness can be usually adjusted varying the speed with which the substrate is removed from the solution. This process was in detail evaluated by Sanchez and colleagues for deposition of thin silica/CTAB films as well as titania/block copolymer mesostructured films by dip-coating.[193] The block-copolymers being responsible for the mesoporous structure formation after their assembly during solvent evaporation and subsequent calcination are usually selected regarding the envisioned mesopore size. On the other hand, block-copolymer assembly and precise synthesis is a vital field which has resulted in various multiblock architectures, bottle brushes, shape readjusting particles, membranes and much more.[194]

Aiming for (nanoscale) step-gradient formation, our research group reported using block-copolymers with suitable functional blocks for *in situ* functionalization in addition to mesopore formation in mesoporous films.[192] As an additional option co-condensation can be used to pre-program functionalization followed by layer-specific post-functionalization. As a first example for *in situ* functionalization Tom *et al.* synthesized amphiphilic PS-*b*-PAA BCPs with different chain lengths and block ratios through single-electron transfer living radical polymerization and applied this block copolymer as a functional template.[195] Multilayer formation was successful and reversible on–off gating for both positive and negative species was achieved. Furthermore, Herzog *et al.* demonstrated the further development of this concept by preparing an amphiphilic polystyrene-*b*-poly(2-vinylpyridine) (PS-*b*-P2VP) and polyferrocenylsilane-*b*-poly(2-vinylpyrindine) (PFS-*b*-P2VP) BCPs with a silane end group and a pH-degradable block (Fig. 5d). Although the silane end-group seems not to be necessary to integrate the BCP into the pore wall, which is attributed to the PEO – tetraethoxysilane (TEOS) interaction, the degradation of the PFS block segment resulted in P2VP-functionalized mesopores with pH-responsive transport performance.[196] Recently, Ngo *et al.* also reported *in situ* polymer functionalization of mesoporous silica through co-condensation of TEOS and a functional polymer with a triethoxysilane terminal group in the presence of poly(ethylene oxide)-*b*-polystyrene (PEO-*b*-PS) used as the pore template.[197] The obtained hybrid material was investigated with respect to its CO_2 gas adsorption capacity with selectivity towards methane and nitrogen.

Modeling studies from the research group of Szleifer pushed this concept of block-copolymers in nanopores towards nanoscale local functionalization including precise copolymer sequence control.[154,155] They proposed a concept for directed and selective ion transport by using a block copolymer with precise sequence design (Fig. 6a–d) including a combination of responsive and nonpolar monomers. These polymers are placed at both pore entrances with nanolocal resolution. Upon consecutive opening and closing of these polymer gates a directed transport is obtained. A theoretical study from Boda and colleagues showed ion distribution for cylindrical nanopores with a charge transition along the length of the nanopore using a multiscale modeling approach.[198] In this study it was observed that the diffusion coefficients are dependent on the net charge of the nanopore although being comparable for charge patterns with the same total charge. Furthermore, ion distribution of monovalent ions follows the charge pattern along the nanopore. An interesting perspective for nanoscale local polymer placement in nanopores going beyond side selective or layer wise design is the use of light or so called maskless lithography or polymer writing approaches comprehensively summarized by Rühe for planar surfaces.[183] In this context the aim is to use light with nanoscale dimensions to induce polymerization or induce hardening. Examples are two photon lithography, scanning near-field optical microscopy (SNOM), or beam pen lithography.[183,199] One potential approach towards nanolocal placement of functional polymers into nanopores is the combination of existing polymerization reactions with nanoscale light sources such as surface plasmons or near field modes in general. In a first proof of concept study our research group demonstrated in 2015[200] that surface plasmons on planar gold surfaces are capable of initiating dye-sensitized polymerizations in mesoporous silica films, inspired by the work of Soppera and colleagues on metal nanoparticles.[201,202] Dye-sensitized polymerizations only offer limited polymerization control but the polymer amount can be adjusted by the irradiation energy and reaction time and they can be combined with basically any plasmon source as an entire library of dyes, and thus initiation wavelengths, are commercially available. Thereby, controlled visible-light iniferterinduced polymerizations[203,204] are a very suitable polymerization reaction allowing polymerization control using grafting through or grafting from polymerizations induced by visible light including surface plasmons in mesoporous films.

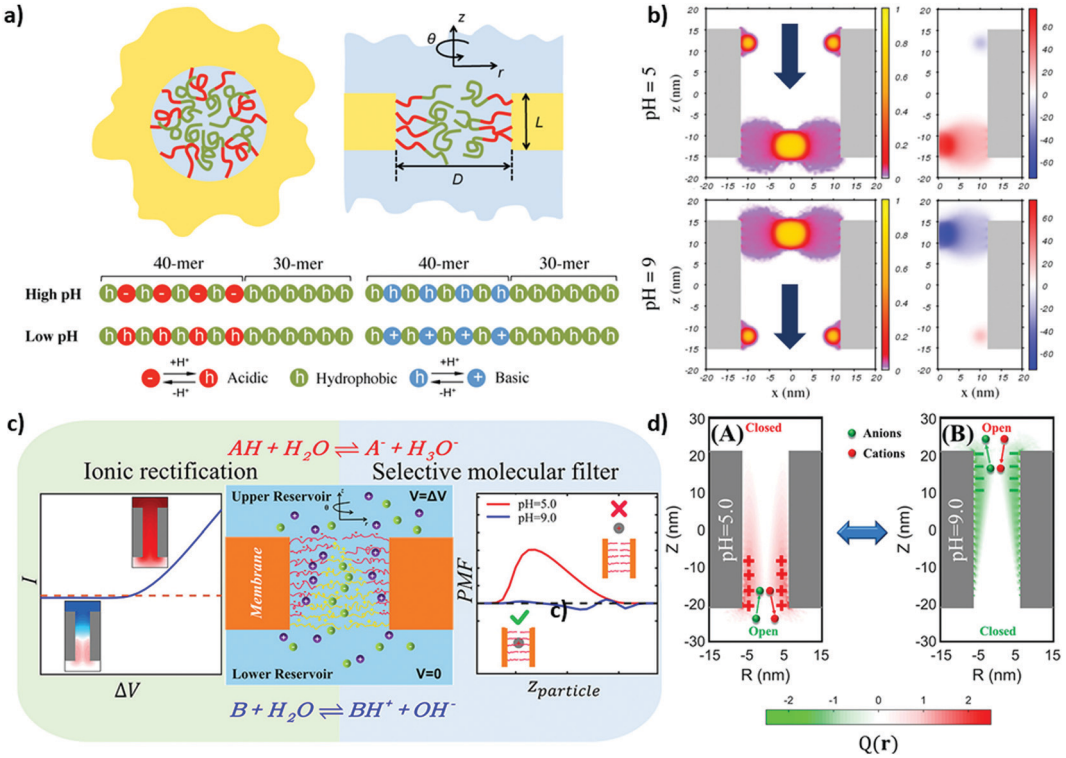

Fig. 6 (a) Schematic representation of the nanopore grafted with a diblock copolymer (polyelectrolyte and hydrophobic blocks are colored in red and green, respectively) along with the sequences of the copolymers with the grafting ends on the left side and the free ends on the right side. (b) Fraction of the polymer volume and the corresponding electrostatic potential of the double-gate nanochannel at different pH values. Reprinted with permission from ref. 155 Copyright (2017), American Chemical Society. (c) Schematic illustration of the nanopore system modified by polyampholyte layers with a composition gradient. (d) The corresponding ion pumping process and the color maps of the charge distribution on the pore axis at different pH values (5 and 9, A and B respectively) at an applied bias of 0.50 V. Reprinted with permission from ref. 154 Copyright (2021), American Chemical Society.

Nanolocal control could be demonstrated embedding plasmonic spherical Ag/Au alloy nanoparticles into mesoporous films.[203] Besides this work on mesoporous films Soppera and colleagues further developed this concept using plasmonic nanoparticles to trigger a photo-ATRP to form a multilayer thin covalent polymer at the surface of the nanostructure with spatial control at the nanoscale.[205] This platform provides a first experimental step towards nanolocal polymer writing and design of nanopore functionalization including the possibility of adjusting polymer composition and chain architecture beyond a layer-wise or step-gradient design and with this towards transport direction, as proposed by Szleifer and colleagues based on nanoscale polymer gates with a highly defined monomer sequence precisely placed into nanopores. However, this platform not only allows nanoscale placement of polymers but can be combined with sensing questions. For example, Liz Marzan as well as Angélomé and colleagues integrate plasmonic nanoparticles into mesoporous films to address sensing questions using surface-enhanced Raman scattering (SERS).[206] This combination can be used in the variety of processes taking place at the confined nanoscale such as sensing and catalysis. Our research group demonstrated that after integration into mesoporous films and nanoscale polymer functionalization refractive index changes are within the average range of detection limits. This can be used to *in situ* follow the polymer formation within mesoporous films limits.[207] The next steps will of course point towards asymmetric plasmonic nanoparticles, their stable integration into mesoporous films and their use for polymer placement and sensing.

Conclusions and outlook

Inspired by the transport performance of biological pores, the fields of nanopore transport control and smart gating have been extensively developed within the last fifteen years aiming to achieve gradual transport, improved transport selectivity, or first examples on transport direction. These advances have been made possible by systematic development of nanopore polymer functionalization as well as recent progress in the design of artificial nanochannels. Although the majority of studies is based on using electrostatic interactions for ionic transport modulation the influence of wettability and ligand binding on transport becomes increasingly recognized. A growing number of publications draws attention to the complex interplay of all these parameters in the confined space of (polymer-) functionalized nanopores. Further pushing the limits of polymer functionalization and precision in material design from the nano to the macroscopic scale bares the potential to approach nature's ability in transport performance. This includes a toolbox of functional building blocks, polymer

location and sequence control, as well as material architecture, and pore composition control in multipore materials. Thereby, the transported species, such as ions, particles, or proteins, has to be considered.

Beyond their investigation and application in transport control these highly defined nanoporous materials help to understand complex porous materials in applications such as chromatography, oil and gas production, or catalysis, for example. This is based on their highly defined structural order and nanopore shape at the nanoscale. Due to this defined structure averaging characterization techniques can be applied to multipore materials still allowing the extraction of information on the nanopore length scale assuming identical nanopores. In addition, single nanopore ion track etched pores allow us to compare such multipore information with the behaviour of individual pores. Although this approach is versatile, improvements in characterization and especially in the local resolution of *in situ* characterization techniques will be needed to further advance toward nature's precision in material design and understanding of transport manipulation.

To bridge the gap between the length scale of material characterization and molecular understanding, modelling is detrimental. In addition, modelling predicts useful material and functionalization parameters to guide the developments in material fabrication and functionalization. Strengthening the interplay of research on new material design and functionalization strategies, high-resolution *in situ* characterization together with modelling will allow us to further implement a so-far unreached transport performance, and integration of nanopores as one element into complex systems. Another tool recently gaining attention in the field of nanopore design and transport is machine learning. Already mentioned in the 2000s,[208] machine learning has received increasing interest since 2017 with strongly increasing numbers of publications up to around twenty in 2021. To date, machine learning in the context of nanopores has been mainly reported in the context of sensing. Examples reach from the identification of amino acids based on their transport through a MoS2 nanopore,[209] to support sensing of viruses[210] as well as biomolecules in conical ion track etched pores[211] or DNA base modifications in so-called oxford nanopore sequencing data,[212] and machine learning is in general investigated for nanopore ionic current blockage classification.[213–215]

When considering all relevant parameters, their interplay and their dynamics a complete picture of the nanopore transport mechanism will enable improvement of existing nanoporous material applications as well as the development of new technologies. For example, controlling the dynamics of nanopore transport to design a nanopore containing out of equilibrium systems is expected to open avenues towards new technologies. One specific example starting to be investigated is ionic circuits in the context of sensing devices.[18,19,216–218]

Future advances will thus strongly depend on increasing precision and complexity in nanopore functionalization, on understanding the interplay of phenomena occurring within nanopores including their kinetics, on the ability to control transport of different species from ions to particles and proteins and on the success of nanopore integration into more complex systems.

Conflicts of interest

There are no conflicts to declare.

Acknowledgements

The authors acknowledge financial support from the European Research Council (ERC) under the European Union's Horizon 2020 research and innovation programme (grant agreement No 803758, 3D-FNPWriting) and from the German Research Foundation (DFG) within the Collaborative Research Centre 1194 ''Interaction between Transport and Wetting Processes'', Project-ID 265191195, subproject C04 as well as from DFG project AN 1301/4. R. P. gratefully acknowledges funding from Career Bridging grant by TU Darmstadt. Adnan Khalil is acknowledged for fruitful discussion in the context of wettability and nanopore transport. A. A.-B. thanks Prof. Wolfgang Knoll and Prof. Ulrich Jonas, for bringing her into contact with polymers and surface plasmon resonance spectroscopy as well as Prof. Omar Azzaroni and Prof. Galo J. A. A. Soler-Illia for their introduction into the fascinating world of nanoporous materials. Prof. Markus Biesalski is acknowledged for his support within the first years at TU-Darmstadt.

References

1 B. Shen, P. Piskunen, S. Nummelin, Q. Liu, M. A. Kostiainen and V. Linko, *ACS Appl. Bio. Mater.*, 2020, **3**, 5606–5619.
2 Z. Zhu, D. Wang, Y. Tian and L. Jiang, *J. Am. Chem. Soc.*, 2019, **141**, 8658–8669.
3 K. K. Unger, R. Ditz, E. Machtejevas and R. Skudas, *Angew. Chem., Int. Ed.*, 2010, **49**, 2300–2312.
4 C. Sanchez, P. Belleville, M. Popall and L. Nicole, *Chem. Soc. Rev.*, 2011, **40**, 696–753.
5 B. M. Venkatesan and R. Bashir, *Nat. Nanotechnol.*, 2011, **6**, 615–624.
6 R. B. Schoch, J. Han and P. Renaud, *Rev. Mod. Phys.*, 2008, **80**, 839–883.
7 Y. He, M. Tsutsui, Y. Zhou and X.-S. Miao, *NPG Asia Mater.*, 2021, **13**, 48.
8 D. A. Doyle, J. Morais Cabral, R. A. Pfuetzner, A. Kuo, J. M. Gulbis, S. L. Cohen, B. T. Cait and R. MacKinnon, *Science*, 1998, **280**, 69–77.
9 R. Y. H. Lim, B. Fahrenkrog, J. Köser, K. Schwarz-Herion, J. Deng and U. Aebi, *Science*, 2007, **318**, 640–643.
10 H. Sui, B.-G. Han, J. K. Lee, P. Walian and B. K. Jap, *Nature*, 2001, **414**, 872–878.
11 Y. A. Perez Sirkin, M. Tagliazucchi and I. Szleifer, *Mater. Today Adv.*, 2020, **5**, 100047.
12 E. Gonzalez Solveyra, R. J. Nap, K. Huang and I. Szleifer, *Polymers*, 2020, **12**, 2282.
13 G. Emilsson, Y. Sakiyama, B. Malekian, K. Xiong, Z. Adali-Kaya, R. Y. H. Lim and A. B. Dahlin, *ACS Cent. Sci.*, 2018, **4**, 1007–1014.
14 M. Tagliazucchi, Y. Rabin and I. Szleifer, *J. Am. Chem. Soc.*, 2011, **133**, 17753–17763.
15 M. Tagliazucchi, O. Azzaroni and I. Szleifer, *J. Am. Chem. Soc.*, 2010, **132**, 12404–12411.
16 G. Sun, S. Senapati and H.-C. Chang, *Lab Chip*, 2016, **16**, 1171–1177.
17 K. Tybrandt, K. C. Larsson, A. Richter-Dahlfors and M. Berggren, *Proc. Natl. Acad. Sci. U. S. A.*, 2010, **107**, 9929–9932.

18 R. A. Lucas, C.-Y. Lin, L. A. Baker and Z. S. Siwy, *Nat. Commun.*, 2020, **11**, 1568.
19 V. Gomez, P. Ramirez, J. Cervera, M. Ali, S. Nasir, W. Ensinger and S. Mafe, *Electrochem. Commun.*, 2018, **88**, 52–56.
20 M. Faustini, D. Grosso, C. Boissière, R. Backov and C. Sanchez, *J. Sol-Gel Sci. Technol.*, 2014, **70**, 216–226.
21 Q. Lei, J. Guo, A. Noureddine, A. Wang, S. Wuttke, C. J. Brinker and W. Zhu, *Adv. Funct. Mater.*, 2020, **30**, 1909539.
22 K. S. W. Sing, *Pure Appl. Chem.*, 1985, **57**, 603–619.
23 H. Daiguji, *Chem. Soc. Rev.*, 2010, **39**, 901–911.
24 G. Pérez-Mitta, A. G. Albesa, C. Trautmann, M. E. Toimil-Molares and O. Azzaroni, *Chem. Sci.*, 2017, **8**, 890–913.
25 S. Alberti, G. J. A. A. Soler-Illia and O. Azzaroni, *Chem. Commun.*, 2015, **51**, 6050–6075.
26 G. J. A. A. Soler-Illia and O. Azzaroni, *Chem. Soc. Rev.*, 2011, **40**, 1107–1150.
27 H. Zhang, Y. Tian and L. Jiang, *Chem. Commun.*, 2013, **49**, 10048–10063.
28 J. Peter, R. Nechikkattu, A. Mohan, A. Maria Thomas and C.-S. Ha, *Mater. Sci. Eng., B*, 2021, **270**, 115232.
29 G. Laucirica, Y. Toum Terrones, V. Cayón, M. L. Cortez, M. E. Toimil-Molares, C. Trautmann, W. Marmisollé and O. Azzaroni, *TrAC, Trends Anal. Chem.*, 2021, **144**, 116425.
30 G. Pérez-Mitta, M. E. Toimil-Molares, C. Trautmann, W. A. Marmisollé and O. Azzaroni, *Adv. Mater.*, 2019, **31**, 1901483.
31 O. Azzaroni and K. H. A. Lau, *Soft Matter*, 2011, **7**, 8709–8724.
32 J. J. Richardson, J. Cui, M. Björnmalm, J. A. Braunger, H. Ejima and F. Caruso, *Chem. Rev.*, 2016, **23**, 14828–14867.
33 M. Ali, B. Yameen, R. Neumann, W. Ensinger, W. Knoll and O. Azzaroni, *J. Am. Chem. Soc.*, 2008, **130**, 16351–16357.
34 M. Nishizawa, V. P. Menon and C. R. Martin, *Science*, 1995, **268**, 700–702.
35 G. Wang, B. Zhang, J. R. Wayment, J. M. Harris and H. S. White, *J. Am. Chem. Soc.*, 2006, **128**, 7679–7686.
36 G. Wang, A. K. Bohaty, I. Zharov and H. S. White, *J. Am. Chem. Soc.*, 2006, **128**, 13553–13558.
37 R. Klajn, *Chem. Soc. Rev.*, 2014, **43**, 148–184.
38 G. Balasubramanian, J. Schulte, F. Müller-Plathe and M. C. Böhm, *Chem. Phys. Lett.*, 2012, **554**, 60–66.
39 F. Krohm, J. Kind, R. D. Savka, M. Alcarez-Janßen, D. Herold, H. Plenio, C. M. Thiele and A. Andrieu-Brunsen, *J. Mater. Chem. C*, 2016, **4**, 4067–4077.
40 T. Ma, M. Walko, M. Lepoitevin, J.-M. Janot, E. Balanzat, A. Kocer and S. Balme, *Adv. Mater. Interfaces*, 2018, **5**, 1701051.
41 Y. Li and T. Ito, *Langmuir*, 2008, **24**, 8959–8963.
42 S. P. Adiga and D. W. Brenner, *Nano Lett.*, 2005, **5**, 2509–2514.
43 O. Schepelina and I. Zharov, *Langmuir*, 2006, **22**, 10523–10527.
44 O. Schepelina, N. Poth and I. Zharov, *Adv. Funct. Mater.*, 2010, **20**, 1962–1969.
45 O. Schepelina and I. Zharov, *Langmuir*, 2007, **23**, 12704–12709.
46 B. Yameen, M. Ali, R. Neumann, W. Ensinger, W. Knoll and O. Azzaroni, *J. Am. Chem. Soc.*, 2009, **131**, 2070–2071.
47 W. Hu, T. Takeuchi and H. Haraguchi, *Anal. Chem.*, 1993, **65**, 2204–2208.
48 C. Xia, X. Fan, J. Locklin, R. C. Advincula, A. Gies and W. Nonidez, *J. Am. Chem. Soc.*, 2004, **126**, 8735–8743.
49 A. Calvo, B. Yameen, F. J. Williams, G. J. A. A. Soler-Illia and O. Azzaroni, *J. Am. Chem. Soc.*, 2009, **131**, 10866–10868.
50 T.-Y. Liu, H.-G. Yuan, Q. Li, Y.-H. Tang, Q. Zhang, W. Qian, B. Van der Bruggen and X. Wang, *ACS Nano*, 2015, **9**, 7488–7496.
51 B. Yameen, M. Ali, R. Neumann, W. Ensinger, W. Knoll and O. Azzaroni, *Nano Lett.*, 2009, **9**, 2788–2793.
52 A. Brunsen, C. Diaz, L. I. Pietrasanta, B. Yameen, M. Ceolin, G. J. A. A. Soler-Illia and O. Azzaroni, *Langmuir*, 2012, **28**, 3583–3592.
53 A. Brunsen, J. Cui, M. Ceolín, A. D. Campo, G. J. A. A. Soler-Illia and O. Azzaroni, *Chem. Commun.*, 2012, **48**, 1422–1424.
54 J. Elbert, F. Krohm, C. Rüttiger, S. Kienle, H. Didzoleit, B. N. Balzer, T. Hugel, B. Stühn, M. Gallei and A. Brunsen, *Adv. Funct. Mater.*, 2014, **24**, 1591–1601.
55 G. Hou, D. Wang, K. Xiao, H. Zhang, S. Zheng, P. Li, Y. Tian and L. Jiang, *Small*, 2018, **14**, 1703369.
56 J. Elbert, M. Gallei, C. Rüttiger, A. Brunsen, H. Didzoleit, B. Stühn and M. Rehahn, *Organometallics*, 2013, **32**, 5873–5878.
57 W. Guo, H. Xia, L. Cao, F. Xia, S. Wang, G. Zhang, Y. Song, Y. Wang, L. Jiang and D. Zhu, *Adv. Funct. Mater.*, 2010, **20**, 3561–3567.
58 R. Brilmayer, C. Hess and A. Andrieu-Brunsen, *Small*, 2019, **15**, 1902710.
59 J. Wang, L. Liu, G. Yan, Y. Li, Y. Gao, Y. Tian and L. Jiang, *ACS Appl. Mater. Interfaces*, 2021, **13**, 14507–14517.
60 M. Li, Y. Xiong, W. Lu, X. Wang, Y. Liu, B. Na, H. Qin, M. Tang, H. Qin, M. Ye, X. Liang and G. Qing, *J. Am. Chem. Soc.*, 2020, **142**, 16324–16333.
61 F. M. Gilles, M. Tagliazucchi, O. Azzaroni and I. Szleifer, *J. Phys. Chem. C*, 2016, **120**, 4789–4798.
62 R. Brilmayer, S. Kübelbeck, A. Khalil, M. Brodrecht, U. Kunz, H.-J. Kleebe, G. Buntkowsky, G. Baier and A. Andrieu-Brunsen, *Adv. Mater. Interfaces*, 2020, 1901914.
63 D. Bottenus, Y.-J. Oh, S. M. Han and C. F. Ivory, *Lab Chip*, 2008, **9**, 219–231.
64 A. Yamaguchi, M. Namekawa, T. Kamijo, T. Itoh and N. Teramae, *Anal. Chem.*, 2011, **83**, 2939–2946.
65 S. Brasselet and W. E. Moerner, *Single Mol.*, 2000, **1**, 17–23.
66 R. Brilmayer, M. Brodrecht, C. Kaiser, H. Breitzke, B. Kumari, J. Wachtveitl, G. Buntkowsky and A. Andrieu-Brunsen, *Chem. Nanostruct. Mater.*, 2020, **6**, 1–12.
67 E. Juère, R. Caillard and F. Kleitz, *Microporous Mesoporous Mater.*, 2020, **306**, 110482.
68 P. Aryal, M. S. P. Sansom and S. J. Tucker, *J. Mol. Biol.*, 2015, **427**, 121–130.
69 J. Haneveld, N. R. Tas, N. Brunets, H. V. Jansen and M. Elwenspoek, *J. Appl. Phys.*, 2008, **104**, 014309.
70 O. Vincent, B. Marguet and A. D. Stroock, *Langmuir*, 2017, **33**, 1655–1661.
71 Q. Yang, P. Z. Sun, L. Fumagalli, Y. V. Stebunov, S. J. Haigh, Z. W. Zhou, I. V. Grigorieva, F. C. Wang and A. K. Geim, *Nature*, 2020, **588**, 250–253.
72 X. Zhang, H. Liu and L. Jiang, *Adv. Mater.*, 2019, **31**, 1804508.
73 S. Utech, K. Bley, J. Aizenberg and N. Vogel, *J. Mater. Chem. A*, 2016, **4**, 6853.
74 K. R. Phillips, G. T. England, S. Sunny, E. Shirman, T. Shirman, N. Vogel and J. Aizenberg, *Chem. Soc. Rev.*, 2016, **45**, 281–322.
75 A. Khalil, M. Zimmermann, A. K. Bell, U. Kunz, S. Hardt, H.-J. Kleebe, R. W. Stark, P. Stephan and A. Andrieu-Brunsen, *J. Colloid Interface Sci.*, 2020, **560**, 369–378.
76 M. Ochs, A. Khalil, T. Frömling and A. Andrieu-Brunsen, *Adv. Mater. Interfaces*, 2021, **8**, 2002095.
77 R. Urteaga, M. Mercuri, R. Gimenez, M. G. Bellino and C. L. A. Berli, *J. Colloid Interface Sci.*, 2019, **537**, 407–413.
78 C. B. Ran, G. Q. Ding, W. C. Liu, Y. T. Deng and W. Hou, *Langmuir*, 2008, **24**, 9952.
79 M. R. Powell, L. Cleary, M. Davenport, K. J. Shea and Z. S. Siwy, *Nat. Nanotechnol.*, 2011, **6**, 798–802.
80 F. Rios and S. N. Smirnov, *Chem. Mater.*, 2011, **23**, 3601–3605.
81 Y. Xue, J. Markmann, H. Duan, J. Weissmüller and P. Huber, *Nat. Commun.*, 2014, **5**, 4237–4245.
82 J. M. Berg, L. G. T. Eriksson, P. M. Claesson and K. G. N. Borve, *Langmuir*, 1994, **10**, 1225–1234.
83 E. A. Vogler, *Adv. Colloid Interface Sci.*, 1998, **74**, 69–117.
84 Y. Tian and L. Jiang, *Nat. Mater.*, 2013, **12**, 291–292.
85 B. Samuel, H. Zhao and K.-Y. Law, *J. Phys. Chem. C*, 2011, **115**, 14852–14861.
86 R. Mani, C. Semprebon, D. Kadau, H. J. Herrmann, M. Brinkmann and S. Herminghaus, *Phys. Rev. E: Stat., Nonlinear, Soft Matter Phys.*, 2015, **91**, 042204.
87 J. Murison, B. Semin, J.-C. Baret, S. Herminghaus, M. Schröter and M. Brinkmann, *Phys. Rev. Appl.*, 2014, **2**, 034002.
88 S. Herminghaus, M. Brinkmann and R. Seemann, *Annu. Rev. Mater. Res.*, 2008, **38**, 101–121.
89 D. Vanzo, D. Bratko and A. Luzar, *J. Phys. Chem. C*, 2012, **116**, 15467–15473.
90 K. R. Phillips, N. Vogel, I. B. Burgess, C. C. Perry and J. Aizenberg, *Langmuir*, 2014, **30**, 7615–7620.
91 I. B. Burgess, N. Koay, K. P. Raymond, M. Kolle, M. Lončar and J. Aizenberg, *ACS Nano*, 2012, **6**, 1427–1437.
92 I. B. Burgess, L. Mishchenko, B. D. Hatton, M. Kolle, M. Lončar and J. Aizenberg, *J. Am. Chem. Soc.*, 2011, **133**, 12430–12432.
93 Y. Yu, S. Brandt, N. J. Nicolas and J. Aizenberg, *ACS Appl. Mater. Interfaces*, 2020, **12**, 1924–1929.

94 J. Groten, C. Bunte and J. Rühe, *Langmuir*, 2012, **28**, 15038–15046.
95 A. Khalil, P. Rostami, G. K. Auernhammer and A. Andrieu-Brunsen, *Adv. Mater. Interfaces*, 2021, **8**, 2100252.
96 G. Xie, P. Li, Z. Zhao, Z. Zhu, X.-Y. Kong, Z. Zhang, K. Xiao, L. Wen and L. Jiang, *J. Am. Chem. Soc.*, 2018, **140**, 4552–4559.
97 H. R. Corti, G. A. Appignanesi, M. C. Barbosa, J. R. Bordin, C. Calero, G. Camisasca, M. D. Elola, G. Franzese, P. Gallo, A. Hassanali, K. Huang, D. Laria, C. A. Menéndez, J. M. M. de Oca, M. P. Longinotti, J. Rodriguez, M. Rovere, D. Scherlis and I. Szleifer, *Eur. Phys. J. E: Soft Matter Biol. Phys.*, 2021, **44**, 136.
98 S. Chattopadhyay, A. Uysal, B. Stripe, Y.-G. Ha, T. J. Marks, E. A. Karapetrova and P. Dutta, *Phys. Rev. Lett.*, 2010, **105**, 037803.
99 M. Shaat, *Langmuir*, 2017, **33**, 12814–12819.
100 K. Wu, Z. Chen, J. Li, X. Li, J. Xu and X. Dong, *Proc. Natl. Acad. Sci. U. S. A.*, 2017, **114**, 3358–3363.
101 P. A. Thompson and M. O. Robbins, *Science*, 1990, **250**, 792–794.
102 Y. Tomo, A. Askounis, T. Ikuta, Y. Takata, K. Sefiane and K. Takahashi, *Nano Lett.*, 2018, **18**, 1869–1874.
103 N. R. Haria, G. S. Grest and C. D. J. J. O. P. C. C. Lorenz, *J. Phys. Chem. C*, 2013, **117**, 6096–6104.
104 O. I. Vinogradova, *Langmuir*, 1995, **11**, 2213–2220.
105 O. Beckstein, P. C. Biggin and M. S. P. Sansom, *J. Phys. Chem. B*, 2001, **105**, 12902–12905.
106 G. Hummer, J. C. Rasaiah and J. P. Noworyta, *Nature*, 2001, **414**, 188–190.
107 C. I. Lynch, S. Rao and M. S. P. Sansom, *Chem. Rev.*, 2020, **120**, 10298–10335.
108 J. L. Trick, P. Aryal, S. J. Tucker and M. S. Sansom, *Biochem. Soc. Trans.*, 2015, **43**, 146–150.
109 M. Pevarnik, K. Healy, M. Davenport, J. Yen and Z. S. Siwy, *Analyst*, 2012, **137**, 2944–2950.
110 D. R. Ceratti, M. Faustini, C. Sinturel, M. Vayer, V. Dahirel, M. Jardat and D. Grosso, *Nanoscale*, 2015, **7**, 5371–5382.
111 W. Lin, S. Xiong, Y. Liu, Y. He, S. Chu and S. Liu, *Phys. Fluids*, 2021, **33**, 032013.
112 H. Hu, Q. Li, S. Liu and T. Fang, *Appl. Surf. Sci.*, 2019, **494**, 249–258.
113 J. Xiao, H. A. Stone and D. Attinger, *Langmuir*, 2012, **28**, 4208–4212.
114 P. Huber, *J. Condens. Matter Phys.*, 2015, **27**, 103102.
115 A. Khalil, F. Schäfer, N. Postulka, M. Stanzel, M. Biesalski and A. Andrieu-Brunsen, *Nanoscale*, 2020, **12**, 24228.
116 M. Mercuri, K. Pierpauli, M. G. Bellino and C. L. A. Berli, *Langmuir*, 2017, **33**, 152–157.
117 C. Boissiere, D. Grosso, S. Lepoutre, L. Nicole, A. B. Bruneau and C. Sanchez, *Langmuir*, 2005, **21**, 12362–12371.
118 R. Valiullin, S. Naumov, P. Galvosas, J. Kärger, H.-J. Woo, F. Porcheron and P. A. Monson, *Nature*, 2006, **443**, 965–968.
119 A. V. Kityk, K. Knorr and P. Huber, *Phys. Rev. B: Condens. Matter Mater. Phys.*, 2009, **80**, 035421.
120 S. Gruener, H. E. Hermes, B. Schillinger, S. U. Egelhaaf and P. J. C. Huber, *Colloids Surf. A: Physicochem. Eng. Asp.*, 2016, **496**, 13–27.
121 M. Boudot, D. R. Ceratti, M. Faustini, C. Boissière and D. Grosso, *J. Phys. Chem. C*, 2014, **118**, 23907–23917.
122 J. W. Polster, E. T. Acar, F. Aydin, C. Zhan, T. A. Pham and Z. S. Siwy, *ACS Nano*, 2020, **14**, 4306–4315.
123 Y. Guillemin, M. Etienne, E. Aubert and A. Walcarius, *J. Mater. Chem.*, 2010, **20**, 6799–6807.
124 O. Azzaroni, A. A. Brown and W. T. S. Huck, *Adv. Mater.*, 2007, **19**, 151–154.
125 L. Silies, E. Gonzalez Solveyra, I. Szleifer and A. Andrieu-Brunsen, *Langmuir*, 2018, **34**, 5943–5953.
126 Z. Chehadi, C. Boissière, C. Chanéac and M. Faustini, *Nanoscale*, 2020, **12**, 13368–13376.
127 R. Gimenez, F. Gonzalez, G. J. A. A. Soler-Illia, C. L. A. Berli and M. G. Bellino, *J. Phys. Chem. B*, 2021, **125**, 1241–1247.
128 M. Thommes, K. Kaneko, A. V. Neimark, J. P. Olivier, F. Rodriguez-Reinoso, J. Rouquerol and K. S. W. Sing, *Pure Appl. Chem.*, 2015, **87**, 1051–1069.
129 Z. Siwy, L. Trofin, P. Kohli, L. A. Baker, C. Trautmann and C. R. Martin, *J. Am. Chem. Soc.*, 2005, **127**, 5000–5001.
130 H. Bayley, O. Braha and L.-Q. Gu, *Adv. Mater.*, 2000, **12**, 139–142.
131 H. Bayley and P. S. Cremer, *Nature*, 2001, **413**, 226–230.
132 M. Tagliazucchi and I. Szleifer, *J. Am. Chem. Soc.*, 2015, **137**, 12539.
133 M. Tagliazucchi and I. Szleifer, *Mater. Today*, 2015, **18**, 131–142.
134 A. Andrieu-Brunsen, S. Micoureau, M. Tagliazucchi, I. Szleifer, O. Azzaroni and G. J. A. A. Soler-Illia, *Chem. Mater.*, 2015, **27**, 808–821.
135 J. E. Basconi, G. Carta and M. R. Shirts, *Langmuir*, 2015, **31**, 4176–4187.
136 M. Kruk, *Isr. J. Chem.*, 2012, **52**, 246–255.
137 R. Brilmayer, C. Förster, L. Zhao and A. Andrieu-Brunsen, *Curr. Opin. Biotechnol*, 2020, **63**, 200–209.
138 J. O. Zoppe, N. Cavusoglu Ataman, P. Mocny, J. Wang, J. Moraes and H.-A. Klok, *Chem. Rev.*, 2017, **117**, 1105–1318.
139 M. Kruk, B. Dufour, E. B. Celer, T. Kowalewski, M. Jaroniec and K. Matyjaszewski, *Macromolecules*, 2008, **41**, 8584–8591.
140 P. Pasetto, H. Blas, F. Audouin, C. Boissiere, C. Sanchez, M. Save and B. Charleux, *Macromolecules*, 2009, **42**, 5983–5995.
141 M. Chen, H. Zhou, L. Zhou and F. Zhang, *Polymer*, 2017, **114**, 180–188.
142 H. Bayat, M. Raoufi, I. Zamrik and H. Schönherr, *Langmuir*, 2020, **36**, 2663–2672.
143 J. Chen, M. Liu, L. Huang, H. Huang, Q. Wan, J. Tian, Y. Wen, F. Deng, X. Zhang and Y. Wei, *J. Taiwan Inst. Chem. Eng.*, 2018, **91**, 570–577.
144 J. Chen, M. Liu, H. Huang, F. Deng, L. Mao, Y. Wen, L. Huang, J. Tian, X. Zhang and Y. Wei, *J. Mol. Liq.*, 2018, **259**, 179–185.
145 J. Tom, R. Brilmayer, J. Schmidt and A. Andrieu-Brunsen, *Polymers*, 2017, **9**, 539.
146 Y. Zheng, Z. M. Abbas, A. Sarkar, Z. Marsh, M. Stefik and B. C. Benicewicz, *Polymer*, 2018, **135**, 193–199.
147 M. Mazurowski, K. Sondergeld, J. Elbert, C. J. Kim, J. Li, H. Frielinghaus, M. Gallei, B. Stühn and M. Rehahn, *Macromol. Chem. Phys.*, 2013, **214**, 1094–1106.
148 C. J. Kim, K. Sondergeld, M. Mazurowski, M. Gallei, M. Rehahn, T. Spehr, H. Frielinghaus and B. Stühn, *Colloid Polym. Sci.*, 2013, **291**, 2087–2099.
149 J. Elbert, J. Mersini, N. Vilbrandt, C. Lederle, M. Kraska, M. Gallei, B. Stühn, H. Plenio and M. Rehahn, *Macromolecules*, 2013, **46**, 4255–4267.
150 K. Eder, E. Reichel, H. Schottenberger, C. G. Huber and M. R. Buchmeiser, *Macromolecules*, 2001, **34**, 4334–4341.
151 R. Bandari, J. Kuballa and M. R. Buchmeiser, *J. Sep. Sci.*, 2013, **36**, 1169–1175.
152 M. R. Buchmeiser, in *Surface-Initiated Polymerization I*, ed. R. Jordan, Springer-Verlag: Berlin, 2006, 197, pp. 137–171.
153 S. Ma, J. Liu, Q. Ye, D. Wang, Y. Liang and F. Zhou, *J. Mater. Chem. A*, 2014, **2**, 8804–8814.
154 S. Qin, K. Huang and I. Szleifer, *ACS Nano*, 2021, **15**, 17678–17688.
155 K. Huang and I. Szleifer, *J. Am. Chem. Soc.*, 2017, **139**, 6422–6430.
156 M. Sadeghi, M. H. Saidi, A. Moosavi and M. Kröger, *J. Phys. Chem. C*, 2020, **124**, 18513–18531.
157 C.-W. Li, H. Merlitz and J.-U. Sommer, *Macromolecules*, 2020, **53**, 6711–6719.
158 C.-W. Li, H. Merlitz, C.-X. Wu and J.-U. Sommer, *Macromolecules*, 2018, **51**, 6238–6247.
159 M. Barsbay, O. Güven, H. Bessbousse, T. L. Wade, F. Beuneu and M.-C. Clochard, *J. Membr. Sci.*, 2013, **445**, 135–145.
160 L. Silies, H. Didzoleit, C. Hess, B. Stühn and A. Andrieu-Brunsen, *Chem. Mater.*, 2015, **27**, 1971–1981.
161 L. Silies and A. Andrieu-Brunsen, *Langmuir*, 2018, **34**, 807–816.
162 Z. Siwy, *Adv. Funct. Mater.*, 2006, **16**, 735–746.
163 Z. Siwy, I. D. Kosińska, A. Fuliński and C. R. Martin, *Phys. Rev. Lett.*, 2005, **94**, 048102.
164 Z. Wang, X. Yang, Z. Cheng, Y. Liu, L. Shao and L. Jiang, *Mater. Horiz.*, 2017, **4**, 701–708.
165 M. Nau, N. Herzog, J. Schmidt, T. Meckel, A. Andrieu-Brunsen and M. Biesalski, *Adv. Mater. Interfaces*, 2019, **6**, 1900892.
166 C. Li, L. Wen, X. Sui, Y. Cheng, L. Gao and L. Jiang, *Sci. Adv.*, 2021, **7**, eabg2183.
167 Y. Izshizaki, S. Yamamoto, T. Miyashita and M. Mitsuishi, *Langmuir*, 2021, **37**, 5627–5634.
168 X. Tian, H. Jin, J. Sainio, R. H. A. Ras and O. Ikkala, *Adv. Funct. Mater.*, 2014, **24**, 6023–6028.
169 Q. Ma, Y. Li, R. Wang, H. Xu, Q. Du, P. Gao and F. Xia, *Nat. Commun.*, 2021, **12**, 1573.
170 X. Lin, Q. Yang, F. Yan, B. Zhang and B. Su, *ACS Appl. Mater. Interfaces*, 2016, **8**, 33343–33349.

171 Q. Yang, X. Lin, Y. Wang and B. Su, *Nanoscale*, 2017, **9**, 18523–18528.
172 Z. Zhang, P. Li, X.-Y. Kong, G. Xie, Y. Qian, Z. Wang, Y. Tian, L. Wen and L. Jiang, *J. Am. Chem. Soc.*, 2018, **140**, 1083–1090.
173 X. Wu, P. Ramiah Rajasekaran and C. R. Martin, *ACS Nano*, 2016, **10**, 4637–4643.
174 K. Xiao, L. Chen, R. Chen, T. Heil, S. D. C. Lemus, F. Fan, L. Wen, L. Jiang and M. Antonietti, *Nat. Commun.*, 2019, **10**, 74.
175 L. Wang, Z. Wang, S. K. Patel, S. Lin and M. Elimelech, *ACS Nano*, 2021, **15**, 4093–4107.
176 G. Laucirica, M. E. Toimil-Molares, C. Trautmann, W. Marmisollé and O. Azzaroni, *Chem. Sci.*, 2021, **12**, 12874–12910.
177 Y. Wu, Y. Qian, B. Niu, J. Chen, X. He, L. Yang, X.-Y. Kong, Y. Zhao, X. Lin, T. Zhou, L. Jiang and L. Wen, *Small*, 2021, **17**, 2101099.
178 P. Apel, Y. E. Korchev, Z. Siwy, R. Spohr and M. Yoshida, *Nucl. Instrum. Methods Phys. Res., Sect. B*, 2001, **184**, 337–346.
179 T. Ma, J.-M. Janot and S. Balme, *Small Methods*, 2020, **4**, 2000366.
180 Z.-Q. Wu, Z.-Q. Li, X.-L. Ding, Y.-L. Hu and X.-H. Xia, *J. Phys. Chem. C*, 2021, **125**, 24622–24629.
181 X. Huang, X.-Y. Kong, L. Wen and L. Jiang, *Adv. Funct. Mater.*, 2018, **28**, 1801079.
182 Z. Zhang, L. Wen and L. J. C. S. R. Jiang, *Chem. Soc. Rev.*, 2018, **47**(2), 322–356.
183 J. Rühe, *ACS Nano*, 2017, **11**, 8537–8541.
184 Z. Nie and E. Kumacheva, *Nat. Mater.*, 2008, **7**, 277–290.
185 I. Vlassiouk and Z. Siwy, *Nano Lett.*, 2007, **7**, 552–556.
186 I. Vlassiouk, T. R. Kozel and Z. Siwy, *J. Am. Chem. Soc.*, 2009, **131**, 8211–8220.
187 X. Hou, F. Yang, L. Li, Y. Song, L. Jiang and D. Zhu, *J. Am. Chem. Soc.*, 2010, **132**, 11736–11742.
188 H. Zhang, Y. Tian, J. Hou, X. Hou, G. Hou, R. Ou, H. Wang and L. Jiang, *ACS Nano*, 2015, **9**, 12264–12283.
189 H. Zhang, X. Hou, L. Zeng, F. Yang, L. Li, D. Yan, Y. Tian and L. Jiang, *J. Am. Chem. Soc.*, 2013, **135**, 16102–16110.
190 A. M. M. Jani, I. M. Kempson, D. Losic and N. H. Voelcker, *Angew. Chem., Int. Ed.*, 2010, **49**, 7933–7937.
191 M. Stanzel, U. Kunz and A. Andrieu-Brunsen, *Eur. Polym. J.*, 2021, **156**, 110604.
192 N. Herzog, R. Brilmayer, M. Stanzel, A. Kalyta, D. Spiehl, E. Dörsam, C. Hess and A. Andrieu-Brunsen, *RSC Adv.*, 2019, **9**, 23570–23578.
193 D. Grosso, F. Cagnol, G. J. D. A. A. Soler-Illia, E. L. Crepaldi, H. Amenitsch, A. Brunet-Bruneau, A. Bourgeois and C. Sanchez, *Adv. Funct. Mater.*, 2004, **14**, 309–322.
194 C. K. Wong, X. Qiang, A. H. E. Müller and A. H. Gröschel, *Prog. Polym. Sci.*, 2020, **102**, 101211.
195 J. C. Tom, C. Appel and A. Andrieu-Brunsen, *Soft Matter*, 2019, **15**, 8077–8083.
196 N. Herzog, H. Hübner, C. Rüttiger, M. Gallei and A. Andrieu-Brunsen, *Langmuir*, 2020, **36**, 4015–4024.
197 T. T. T. Ngo, E. Besson, E. Bloch, S. Bourrelly, R. Llewellyn, S. Gastaldi, P. L. Llewellyn, D. Gigmes and T. N. T. Phan, *Microporous Mesoporous Mater.*, 2021, **319**, 111036.
198 M. Valiskó, B. Matejczyk, Z. Ható, T. Kristóf, E. Mádai, D. Fertig, D. Gillespie and D. Boda, *J. Chem. Phys.*, 2019, **150**, 144703.
199 A. I. Ciuciu and P. J. Cywinski, *RSC Adv.*, 2014, **4**, 45504–45516.
200 N. Herzog, J. Kind, C. Hess and A. Andrieu-Brunsen, *Chem. Commun.*, 2015, **51**, 11697–11700.
201 C. Deeb, C. Ecoffet, R. Bachelot, J. Plain, A. Bouhelier and O. Soppera, *J. Am. Chem. Soc.*, 2011, **133**, 10535–10542.
202 H. Ibn-El-Ahrach, R. Bachelot, G. Lérondel, A. Vial, A.-S. Grimault, J. Plain, P. Royer and O. Soppera, *J. Microsc.*, 2008, **229**, 421–427.
203 D. John, M. Stanzel and A. Andrieu-Brunsen, *Adv. Funct. Mater.*, 2021, **31**, 2009732.
204 D. John, R. Mohammadi, N. Vogel and A. Andrieu-Brunsen, *Langmuir*, 2020, **36**, 1671–1679.
205 F. Kameche, W. Heni, S. Telitel, D. Ge, L. Vidal, F. Dumur, D. Gigmes, J. Lalevée, S. Marguet, L. Douillard, C. Fiorini-Debuisschert, R. Bachelot and O. Soppera, *Mater. Today*, 2020, **40**, 38–47.
206 M. M. Zalduendo, V. Oestreicher, J. Langer, L. M. Liz-Marzán and P. C. Angelomé, *Anal. Chem.*, 2020, **92**, 13656–13660.
207 M. Stanzel, L. Zhao, R. Mohammadi, R. Pardehkhorram, U. Kunz, N. Vogel and A. Andrieu-Brunsen, *Anal. Chem.*, 2021, **93**, 5394–5402.
208 S. Winters-Hilt and M. Akeson, *DNA Cell Biol.*, 2004, **23**, 675–683.
209 A. Barati Farimani, M. Heiranian and N. R. Aluru, *npj 2D Mater. Appl.*, 2018, **2**, 14.
210 A. Arima, M. Tsutsui, T. Washio, Y. Baba and T. Kawai, *Anal. Chem.*, 2021, **93**, 215–227.
211 N. Meyer, J.-M. Janot, M. Lepoitevin, M. Smietana, J.-J. Vasseur, J. Torrent and S. Balme, *Biosensors*, 2020, **10**, 140.
212 Q. Liu, L. Fang, G. Yu, D. Wang, C.-L. Xiao and K. Wang, *Nat. Commun.*, 2019, **10**, 2449.
213 Á. D. Carral, M. Ostertag and M. Fyta, *J. Chem. Phys.*, 2021, **154**, 044111.
214 H. Ma and Y.-L. Ying, *Curr. Opin. Electrochem.*, 2021, **26**, 100675.
215 C. Wen, D. Dematties and S.-L. Zhang, *ACS Sens.*, 2021, **6**, 3536–3555.
216 P. Ramirez, V. Garcia-Morales, V. Gomez, M. Ali, S. Nasir, W. Ensinger and S. Mafe, *Phys. Rev. Appl.*, 2017, **7**, 064035.
217 R. A. Lucas and Z. S. Siwy, *ACS Appl. Mater. Interfaces*, 2020, **12**, 56622–56631.
218 M. Ali, P. Ramirez, S. Nasir, J. Cervera, S. Mafe and W. Ensinger, *Soft Matter*, 2019, **15**, 9682–9689.